Nonhydrostatic and surfbeat model predictions of extreme wave run-up in fringing reef environments

Lashley, Chris; Roelvink, D.; Van Dongeren, Ap R.; Buckley, Mark; Lowe, Ryan J.

DOI
10.1016/j.coastaleng.2018.03.007

Publication date
2018

Document Version
Accepted author manuscript

Published in
Coastal Engineering

Citation (APA)
Lashley, C., Roelvink, D., Van Dongeren, A. R., Buckley, M., & Lowe, R. J. (2018). Nonhydrostatic and surfbeat model predictions of extreme wave run-up in fringing reef environments. *Coastal Engineering*, *137*, 11-27. https://doi.org/10.1016/j.coastaleng.2018.03.007

NONHYDROSTATIC AND SURFBEAT MODEL PREDICTIONS OF EXTREME WAVE RUN-UP IN FRINGING REEF ENVIRONMENTS

1. Christopher H. Lashley [a,1]
2. Dano Roelvink [a, b]
3. Ap van Dongeren [b]
4. Mark L. Buckley [c]
5. Ryan J. Lowe [d]

a) Coastal Systems, Engineering & Port Development Chair Group, IHE-Delft Institute for Water Education, Delft, Netherlands.
b) Department of Applied Morphodynamics, Unit of Marine and Coastal Systems, Deltares, Delft, the Netherlands
c) Pacific Coastal and Marine Science Center, U. S. Geological Survey, Santa Cruz, California, USA
d) School of Earth Sciences, The Oceans Institute, and ARC Centre of Excellence for Coral Reef Studies, University of Western Australia, Crawley, Western Australia, Australia

Corresponding author: Christopher H. Lashley (C.H.Lashley@tudelft.nl)

Keywords: Wave run-up, Coral reefs, XBeach, Infragravity waves, Numerical modelling, Coastal flooding

Abstract

The accurate prediction of extreme wave run-up is important for effective coastal engineering design and coastal hazard management. While run-up processes on open sandy coasts have been reasonably well-studied, very few studies have focused on understanding and predicting wave run-up at coral reef-fronted coastlines. This paper applies the short-wave resolving, Nonhydrostatic (XB-NH) and short-wave averaged, Surfbeat (XB-SB) modes of the XBeach numerical model to validate run-up using data from two 1D (alongshore uniform) fringing-reef profiles without roughness elements, with two objectives: i) to provide insight into the physical processes governing run-up in such environments; and ii) to evaluate the performance of both modes in accurately predicting run-up over a wide range of conditions. XBeach was calibrated by optimizing the maximum wave steepness parameter *(maxbrsteep)* in XB-NH and the

[1] Present address: Department of Hydraulic Engineering, Faculty of Civil Engineering and Geosciences, Delft University of Technology, Delft, the Netherlands.

dissipation coefficient (*alpha)* in XB-SB) using the first dataset; and then applied to the second dataset for validation. XB-NH and XB-SB predictions of extreme wave run-up (R_{max} and $R_{2\%}$) and its components, infragravity- and sea-swell band swash (S_{IG} and S_{SS}) and shoreline setup ($<\eta>$), were compared to observations. XB-NH more accurately simulated wave transformation but under-predicted shoreline setup due to its exclusion of parameterized wave-roller dynamics. XB-SB under-predicted sea-swell band swash but overestimated shoreline setup due to an over-prediction of wave heights on the reef flat. Run-up (swash) spectra were dominated by infragravity motions, allowing the short-wave (but not wave group) averaged model (XB-SB) to perform comparably well to its more complete, short-wave resolving (XB-NH) counterpart. Despite their respective limitations, both modes were able to accurately predict R_{max} and $R_{2\%}$.

1 Introduction

Wave run-up is defined as the uprush of water above the still water level (SWL) on a beach or structure. Run-up is the result of two nearshore processes: i) the time-averaged surface elevation at the shoreline (i.e. wave setup); and ii) the time-varying fluctuations about that mean (i.e. swash) [1,2]. Its accurate prediction is essential for the effective design of coastal structures, beach nourishment planning and for predicting the extent of damage associated with storms [3,4].

Accurately predicting run-up is especially important for tropical and sub-tropical regions fronted by reef structures. These regions, which often have low-lying coastal areas, are often threatened by severe tropical storms with impacts ranging from severe beach and dune erosion to the complete inundation of the adjacent coastal communities [5-7]. Coastal inundation is often a result of several interacting meteorological and coastal processes; however, on steeper coasts without continental shelves, the contribution of wave processes such as run-up becomes more dominant than that due to storm surge [8,9].

Coastal engineers and managers typically parameterise run-up using Iribarren-based empirical models (Equations (1) and (2)) developed for open, sandy coasts which use offshore wave height (H_{m0}), period (T_p) and a constant beach slope (β) as input values to predict the magnitude of run-up [10-12,2]. These relationships typically quantify extreme wave run-up as either of two characteristic values: i) R_{max}, the maximum run-up at any specific time; and ii) $R_{2\%}$, the value exceeded by only 2% of the run-up maxima in the distribution.

$$\frac{R_{max}}{H_{m0}} \text{ or } \frac{R_{2\%}}{H_{m0}} = f(\xi_0) \quad \textbf{(1)}$$

$$\xi_0 = \frac{tan\beta}{\sqrt{\frac{2\pi H_{m0}}{gT_p^2}}} \quad \textbf{(2)}$$

where, g is the gravitational acceleration and ξ_0 is the Iribarren number.

However, these formulations are not readily applicable to the fringing reef environments commonly found in tropical and subtropical regions, as run-up depends not only on the beach slope at the shoreline but also on the reef morphology itself. The presence of these reef structures results in significantly more complex nearshore hydrodynamic processes than on typical sandy profiles [13,14,5,7]. Fringing reefs are characterized by a seaward sloping reef face leading up to a shallow reef flat platform that extends towards the beach. Wave transformation in these environments is subject to several simultaneous and interacting processes [15], which include: shoaling; dissipation by wave breaking [16]; wave-induced setup [5,17]; nonlinear energy transfer to higher and/or lower (infragravity) frequencies [18-20]; dissipation by bottom friction [21]; low-frequency wave reflection; and resonance [22], where a significant amount of wave energy is distributed about the natural frequency of the reef. This reef flat resonance may in turn result in an amplification of run-up at the shoreline, further adding to the complexity of making accurate predictions in such environments [23-26].

Although not originally developed for and tested using reef-type environments, numerical models are now widely applied to reef systems given their ability to accurately represent complex nearshore processes [27-32,26]. These numerical models generally fall into two categories groups: i) phase-resolving models and ii) phase-averaged models. Phase-resolving models utilize a grid resolution high enough to completely describe the sea-surface and resolve individual waves. These models are then able to capture the higher frequency wave motions (short-waves); however, this comes at greater computational expense. In contrast, phase-averaged models describe wave processes in a stochastic manner, typically based on linear wave theory and empirical formulations. As such, phase-averaged models require a lower grid resolution and are considerably less computationally demanding [33]. Nearshore wave models have been primarily developed for mild-sloping, sandy coastal environments. Thus, when they are applied to steep reef environments it is expected that some of their inherent parameterizations (e.g. for simulating wave breaking and frictional dissipation) would require some adjustment [33]. However, wave transformation models derived using the mild-slope

approximation have been shown to perform reasonably accurately with minimal parameter tuning, even on slopes up to 1:3, which is steeper than typical coral reef slopes (e.g. [34-36]).

Therefore, the choice of numerical model should be carefully considered based on the relative importance of the wave processes and the manner in which they are simulated in each model. Given that low-frequency motions often dominate near the shoreline of fringing reef environments, it is imperative that the numerical model applied be able to correctly describe the non-linear transfer of wave energy to the infragravity (low-frequency) band [28,33,20]. For this study, we consider the XBeach numerical model that combines both phase-resolving and phase-averaged approaches. The XBeach nonhydrostatic mode (XB-NH) resolves all wave motions including short-waves; while the surfbeat mode (XB-SB) resolves long-wave motions but is short-wave averaged. The overall ability of XBeach to accurately simulate infragravity motions in a wide range of coastal environments has been demonstrated in many studies [37-41].

With respect to its application to fringing reef systems, Van Dongeren et al. [30] applied XB-SB to study low-frequency wave dynamics over a fringing reef at field scales. The study showed the increasing dominance of infragravity (low-frequency) waves shoreward of the reef crest. In their comparison of nearshore models for wave transformation across reef environments, Buckley et al. [33] concluded that XB-SB was indeed capable of handling the transformation of wave energy from the sea-swell (high-frequency) band to the infragravity band. More recently, Quataert et al. [42] applied XB-SB to investigate the influence of the reef characteristics on the nearshore hydrodynamics and the potential for wave-driven flooding in light of climate-driven sea level rise. This study found that run-up increased with narrower, smoother reef flats and steeper, rougher reef slopes. While highly informative, the main limitation of their study was the fact that their model was not quantitatively validated for wave run-up. While each of the above-mentioned studies applied XB-SB, Storlazzi et al. [43] recently used the short-wave resolving mode XB-NH to successfully simulate sea-swell band wave run-up and flooding on an atoll island. However, like that of Quataert et al. [42], the modelled run-up and associated inundation extent were only qualitatively compared to observations. Likewise, Pearson et al. [44] concluded that XB-NH was able to simulate reef hydrodynamics with reasonable accuracy and recommended its use as an early warning tool to predict flooding on reef-lined coasts.

Despite the promising results displayed by XBeach to-date, the performance of either mode to predict wave run-up at reef coasts has not been rigorously validated using experimental data. Thus, it is primary aim of the present paper to evaluate the model in simulating extreme wave run-up in such systems. In particular, attention is given to the physical processes that need to be captured for accurate run-up predictions. This is done by comparing both the short-wave resolving and short-wave averaged modes of the model to two laboratory (physical model) experiments carried out in large-scale wave flumes by: i) Demirbilek et al. [24]; and ii) Buckley et al. [17].

In Section 2, the experiments used for model-data comparison are described, followed by a brief overview of the XBeach numerical model and the equations pertinent to this study. In addition, the metrics and objective functions used to quantify model accuracy are presented. Section 3 presents the results of the model calibration through its application to the Demirbilek et al. [24] dataset; while Section 4 presents the results of the model validation and application to the Buckley et al. [17] dataset. Section 5 provides an in-depth discussion on the performance of the short-wave resolving and short-wave averaged modes; and examines the contribution of various physical processes to model results. Section 6 concludes the paper by addressing the overarching research objective and making recommendations for future studies.

2 Methods

2.1 Description of the Experiments

2.1.1 Demirbilek et al. [24] Experiment

The experiment was conducted in a 35-m long, 0.7-m wide and 1.6-m high wave flume at the University of Michigan. The reef platform was constructed from polyvinyl chloride (PVC) with a composite reef slope (1:5; 1:18.8; 1:10.6), a 4.8-m wide reef flat and a 1:12 beach slope (Figure 1). Applying a geometric scaling of 1:64, this reef flat width of 307 m in field (prototype) scale is a proxy for a typical fringing reef on southeast coast of Guam [24]. The flume generated irregular waves with a plunger-type wave maker which corresponded to a JONSWAP-type spectrum with a peak enhancement factor of 3.3. The experiments under consideration comprised of 29 tests without wind generation and with significant wave heights (H_{m0}) varying from 3.2 to 8.5 cm, spectral peak periods (T_p) from 1 to 2.5s, and still-water depths on the reef flat (h_r) from 0 to 5.1 cm. Water-surface elevations were measured using 8 capacitance-wire wave gauges, all synchronously sampling at 20 Hz for 900 s. Wave run-up

was measured using a 1-m long capacitance wire gauge installed on the beach slope. A summary of the 29 test conditions is provided in Table 1.

2.1.2 Buckley et al. [17] Experiment

The experiment was carried out in the 55-m long Eastern Scheldt wave flume located at Deltares, the Netherlands. The reef profile was built using marine plywood to form a 1:5 reef slope, a 14-m horizontal reef flat and a 1:12 sloping beach (Figure 1). Using a geometric scaling of 1:36, the experimental set-up corresponds to a 500-m long reef flat in field (prototype) scale which is analogous to coral reef flats found globally [17]. Irregular waves were generated with a TMA-type spectrum using a piston-type wave maker with second-order wave generation and active reflection compensation for any offshore directed waves. The experiment consisted of 16 tests with h_r varying from 0 to 9 cm, H_{m0} from 4 to 24 cm and T_p from 1.3 to 2.3 s. Water-surface elevations were measured using resistance gauges positioned at 18 locations sampled synchronously at 40 Hz for 42 minutes (2520 s). Wave run-up was measured using a "wave rake" equipped with vertical sensors positioned along the beach slope [45,46]. The apparatus recorded the position of the highest wet sensor point during each run-up event. It should be noted that the sensors had a horizontal resolution of 2.5 cm for the first 100 cm and a resolution of 5 cm for the remaining 120 cm. A summary of the 16 test conditions is provided in Table 2.

2.2 The XBeach Numerical Model

XBeach is an open-source, two-dimensional numerical model in the horizontal plane (2DH) which solves horizontal equations for wave propagation, long waves and mean flow, sediment transport and morphological changes [37]. The model has two main modes: i) Nonhydrostatic (XB-NH) which resolves all wave motions (short-wave resolving); however, at a more significant computational expense; and ii) Surfbeat (XB-SB) that resolves motions on the scale of wave groups but treats short-wave motions in a phase-averaged manner (short-wave averaged), requiring considerably less computational effort. It should be noted that although XB-SB mode does not resolve sea-swell frequency motions, it does compute steady setup, (un)steady currents and infragravity wave motions, which tend to dominate during extreme (dissipative) events and in fringing reef environments [37,18,47].

XB-NH computes depth-averaged flow due to waves and currents using the non-linear shallow water equations (Equations (3) and (4)). It also includes a nonhydrostatic pressure correction which is derived in a manner similar to a one-layer version of the SWASH model [48]. In the present study, we apply the 1D equations; however, as noted above, 2DH is possible:

$$\frac{\partial \eta}{\partial t} + \frac{\partial uh}{\partial x} = 0 \quad \textbf{(3)}$$

$$\frac{\partial u}{\partial t} + u\frac{\partial u}{\partial x} - v_h \frac{\partial^2 u}{\partial x^2} = -\frac{1}{\rho}\frac{\partial(\bar{q} + \rho g \eta)}{\partial x} - c_f \frac{u|u|}{h} \quad \textbf{(4)}$$

where x and t are the horizontal spatial and temporal coordinates, respectively, η is the free surface elevation, u is the depth-averaged cross-shore velocity, v_h is the horizontal viscosity (following Smagorinsky [49]), h is the local water depth, ρ is the density of water, $\bar{q}$ is the depth-averaged dynamic (nonhydrostatic) pressure normalised by the density and c_f is the bed friction factor. In the present study we obtain the friction factor using the Manning's roughness coefficient, n:

$$c_f = \frac{n^2 g}{\sqrt[3]{h}} \quad \textbf{(5)}$$

XB-NH incorporates depth-limited wave breaking with a shock-capturing momentum conservation scheme but as a depth-integrated model, it does not explicitly simulate overturning or plunging breakers; that is, the vertical structure of flow is not taken into account. To control the computed location and magnitude of wave breaking a hydrostatic front approximation is applied where the pressure distribution under breaking bores is assumed to be hydrostatic [50]. Following Smit et al. [51], the model considers waves to be hydrostatic bores (i.e. the nonhydrostatic pressure correction term ($\overline{q}$) is turned off, see Equation (4)) if the local surface steepness ($\delta\eta/\delta t$) exceeds a maximum value (the "*maxbrsteep*" parameter, by default = 0.6) and this persists until $\delta\eta/\delta t$ is less than a specified secondary steepness value (the "*secbrsteep*" parameter, by default is equal to half the specified *maxbrsteep* value). Higher *maxbrsteep* values allow for steeper wave faces prior to wave-breaking and shifts the breakpoint shoreward.

XB-SB solves short-wave motions using the wave-action equation with time-dependent forcing, similar to that of the HISWA model [52]. XB-SB uses a single representative frequency and the wave-action equation (Equation (6)) is applied at the timescale of the wave group.

$$\frac{\partial A}{\partial t} + \frac{\partial c_{gx} A}{\partial x} = -\frac{D_w}{\sigma} \quad \textbf{(6)}$$

$$A(x,t) = \frac{S_w(x,t)}{\sigma(x,t)} \quad \textbf{(7)}$$

$$\sigma = \sqrt{gk\ tanh\ kh} \quad \textbf{(8)}$$

The wave action, A is calculated by Equation (7) where S_w is the wave energy density, σ is the intrinsic wave frequency (Equation (8)), h is the local water depth and k is the wave number; while, D_w is a dissipation term to account for wave breaking; and c_{gx} is the wave-action propagation speed in the x direction.

To simulate wave breaking, XB-SB applies a dissipation model [53] for use with short-wave groups and a roller model [54,55] to represent momentum stored in surface rollers which cause a shoreward delay in wave forcing. The radiation stress gradients that result from these variations in wave action exert forces on the water column that give rise to infragravity waves, unsteady currents and wave setup which are obtained by solving the non-linear shallow water equations (Equations (3) and (4)) but in hydrostatic form with a short wave-induced force term derived from the wave-action balance (Equation (6)); thus, in a phase-resolving manner. The total wave energy dissipation due to wave breaking, $\overline{D_w}$ (Equation (9)) is determined by a representative wave period, T_{rep}; the fraction of breaking waves, Q_b; the wave-group varying short-wave energy, E_w; the root-mean-square wave height, H_{rms}; water depth, h; and a calibration coefficient for dissipation, α (*alpha*, by default = 1).

$$\overline{D_w} = 2\frac{\alpha}{T_{rep}} Q_b E_w \frac{H_{rms}}{h} \quad \textbf{(9)}$$

$$Q_b = 1 - \exp\left(-\left(\frac{H_{rms}}{H_{max}}\right)^n\right),\ H_{rms} = \sqrt{\frac{8E_w}{\rho g}},\ H_{max} = \gamma h \quad \textbf{(10)}$$

where n is a coefficient (by default = 10); H_{max} is the maximum wave height; and γ is the breaker parameter (by default = 0.55).

Calibration of the above wave dissipation model (Roelvink, 1993, Equations (9 and 10)) may be achieved by varying either of two free parameters: (i) *gamma* (γ), which controls the fraction of breaking waves, Q_b; however, this is only until $H_{rms}/h > 0.6$, after which $Q_b = 1$ and varying *gamma* no longer has an effect (as per Equation (10)); and ii) *alpha* (α), a proportionality parameter which controls the intensity of breaking and represents the magnitude of energy dissipation for a given Q_b. Typically for spilling breakers ($\xi_0 < 0.5$, Equation (2); (Battjes, 1974)), γ is varied and α is expected to be of the order 1. However, given the plunging nature ($0.5 > \xi_0 < 3.3$, Table 1, Table 2) of the waves observed during the physical experiments, we choose to calibrate the XB-SB model using the *alpha* parameter. In general, higher *alpha* values result in increased wave dissipation.

The only change to the published version of XBeach that was made as part of this present study was the inclusion of a TMA spectral wave boundary condition to match the offshore waves produced during Buckley et al. [17] experiment. This modification was achieved by applying the following transformation function, φ to the calculated JONSWAP spectrum [56]:

$$\varphi(f,h) = \frac{1}{2r} tanh^2(kh) \quad \textbf{(11)}$$

where r is the ratio of group velocity to phase velocity. This option is now available in the "XBeachX" release of November, 2017.

2.3 Data Processing and Performance Metrics

In order to assess model performance, the following wave characteristics and near-shore processes were investigated. It should be noted that all data processing (for both the physical experiment and numerical model results) was carried out by excluding the initial spin-up time to ensure steady-state conditions on the reef flat, which were identified by examining the measured time-series. This spin-up time was 100 s for the Demirbilek et al. [24] experiment (leading to a total simulation period of 900 s per case) and 480 s for that of Buckley et al. [17] (total simulation period of 2520 s per case).

2.3.1 Mean water level

The mean water level, $\bar{\eta}$ was calculated by taking the average of the surface elevation time series at each instrument location , relative to SWL.

2.3.2 Root-mean-square wave height

The surface elevation time series were used to determine the one-dimensional wave energy spectra, $C_{\eta\eta}(f)$ by applying the Welch's average periodogram method and Hanning filter with a 50% maximum overlap. For the observations and the XB-NH results, the total root-mean-square wave height, $H_{rms,TOT}$ was then determined as follows:

$$H_{rms,TOT} = \sqrt{8 \int_0^\infty C_{\eta\eta} df} \quad \textbf{(12)}$$

XB-SB uses a representative frequency for the sea-swell band wave energy and does not produce the sea-swell band spectra. Therefore, the high-frequency (sea-swell band) root-mean-square wave height, $H_{rms,SS}$ as computed by the model was used. The low-frequency (infragravity-band) root-mean-square wave height, $H_{rms,IG}$ was then obtained from the variance

of the simulated long-wave surface elevation time series using Equation (12). The modelled total wave height $H_{rms,TOT}$ was then calculated as follows:

$$H_{rms,TOT} = \sqrt{H_{rms,SS}^2 + H_{rms,IG}^2} \quad \textbf{(13)}$$

For this research a split frequency equal to half the peak frequency ($f_{split} = f_p/2$) is considered for the separation of sea-swell and infragravity bands, following [57]. This choice of split frequency is based on the tendency that, offshore, the majority of sea-swell band energy > $f_p/2$, while most of the bound long-wave (infragravity band) energy < $f_p/2$. Combining the two spectra results in a minimum of spectral density around $f_p/2$ separating the high- and low-frequency peaks, which is consistent with the observations here (Figure 4 and Figure 10).

2.3.3 Run-up

Wave run-up is commonly described by the value exceeded by only 2% of the values in the run-up distribution ($R_{2\%}$). This statistic was extracted by applying the local peak method to both modelled and observed run-up time series [58]. Due to the relatively high sampling frequency, the individual run-up maxima (peaks) above the SWL were identified by assessing whether or not each data point was significantly larger than the points around it based on a specified threshold value (Figure 2). $R_{2\%}$ was then determined from the cumulative distribution function of the discrete run-up maxima [2]. Maximum run-up, R_{max} was determined by finding the maximum of the run-up peaks (relative to SWL). The steady setup at the shoreline, $<\eta>$ was obtained by taking the mean of the modelled and observed run-up time series (relative to SWL) [1,58,2]. Note that a distinction is made here between $\bar{\eta}$, the mean water level offshore and over the reef profile; and $<\eta>$, the mean water level at the shoreline obtained from the run-up time series.

Swash motions were obtained from the modelled and observed run-up time series as the time-varying vertical fluctuations at the shoreline (relative to $<\eta>$). Significant swash in both the sea-swell (S_{SS}) and infragravity- (S_{IG}) bands were obtained from the swash energy spectra [1,2]:

$$S_{SS} = 4\sqrt{\int_{fsplit}^{\infty} C_{\eta\eta}\,df} \quad \text{and} \quad S_{IG} = 4\sqrt{\int_{0}^{fsplit} C_{\eta\eta}\,df} \quad \textbf{(14)}$$

2.4 Objective Functions

The model-data comparisons of the above-mentioned performance metrics were carried out by applying the following objective functions: Root-Mean-Square Error (RMSE) (Equation (15)); Scatter Index (SCI) (Equation (16)); and Relative Bias (Equation (17)). In the following equations, Ψ is used as a stand-in for $\bar{\eta}$, $H_{rms,TOT}$, R_{max}, $R_{2\%}$,$<\eta>$, S_{SS} *and* S_{IG}, in a sample size N:

$$RMSE = \sqrt{\frac{1}{n}\sum_{i=1}^{N}\left(\Psi_{XBeach}^{i} - \Psi_{observed}^{i}\right)^{2}} \quad \textbf{(15)}$$

$$SCI_{\Psi} = \frac{\sqrt{\frac{1}{n}\sum_{i=1}^{N}\left(\Psi_{XBeach}^{i} - \Psi_{observed}^{i}\right)^{2}}}{\frac{1}{n}\sum_{i=1}^{N}\Psi_{observed}^{i}} \quad \textbf{(16)}$$

$$Rel.bias_{\Psi} = \frac{\sum_{i=1}^{N}(\Psi_{XBeach}^{i} - \Psi_{observed}^{i})}{\sum_{i=1}^{N}\Psi_{observed}^{i}} \quad \textbf{(17)}$$

3 Model Calibration: Application to Demirbilek et al. [24] Experiment

In this section the XBeach model is calibrated for fringing reef environments by applying it to the Demirbilek et al. [24] dataset and optimizing the key parameters in both XB-NH and XB-SB. This was achieved by minimizing the combined root-mean-square error ($RMSE_{TOT}$) which considers both $H_{rms,TOT}$ and $\bar{\eta}$ predictions at the 8 gauge locations (Equation (18)).

$$RMSE_{TOT} = RMSE_{Hrms,TOT} + RMSE_{MWL} \quad \textbf{(18)}$$

The choice to calibrate the model considering both $H_{rms,TOT}$ and $\bar{\eta}$ predictions aims to ensure that the model's accuracy in predicting either parameter is not improved at the expense of the other. This was observed by Buckley et al. [33] in their evaluation of various nearshore numerical models for reef environments. In that study it was shown how optimizing a model considering $H_{rms,SS}$ alone can often result in an increase in error in $H_{rms,IG}$ and $\bar{\eta}$ predictions.

3.1 Numerical Model Setup

The numerical simulations were configured using a 1D approach to best represent the actual flume conditions. For the XB-NH simulations, a uniform horizontal grid size, Δx of 2.5 cm was

applied; while Δx was allowed to vary from 2.5 cm at the beach slope to 5 cm offshore for the XB-SB simulations. It should be noted that for the stated grid resolutions, the two modes had comparable run times. Both modes were forced with parametric JONSWAP spectra and initial water-levels at the offshore boundary to match those observed during the experiments (Table 1). The model run-time for both modes was set to 900 s with outputs at 20 Hz at each gauge location to match the experimental data. Additionally, bottom friction was specified using a Manning coefficient, n = 0.01 s/m$^{1/3}$ (Equation (5)) to represent the relatively smooth plastic bottom as recommended by Zijlema [59] in his analysis of the same case. A numerical run-up gauge was specified to track the moving waterline with a minimum depth for the determination of the last wet point, *rugdepth* of 0.2 cm to represent the sensitivity of the capacitance wire used during the physical experiment.

Numerical simulations were first carried out using default values to provide an estimate of model performance prior to calibration. For calibration, the key model parameters governing wave dissipation by breaking were identified as: i) the maximum breaking wave steepness in XB-NH (*maxbrsteep*); and ii) the wave dissipation coefficient in XB-SB (*alpha*) (Section 2.2).

For each test, these two parameters were then systematically varied over the range of physically acceptable values [60]. The *maxbrsteep* parameter was varied from 0.3 to 0.8 and *alpha* from 0.5 to 2.0; both in increments of 0.05. Calibration was achieved by minimizing $RMSE_{TOT}$ (Equation (18)) and finding the optimal parameter values. These optimal parameter values and the reduction in error compared to results with default values ($\Delta RMSE_{Hrms,TOT}$) are summarized for all runs in Table 1.

3.2 Wave Transformation

With default parameters, both XBeach modes correctly simulated the wave heights offshore (Gauges 1 – 3, see Figure 1 for gauge locations); however, XB-NH slightly overestimated $H_{rms,TOT}$ in the shoaling region (Gauges 4 and 5) for the majority of the tests simulated (Figure 3). Likewise, $H_{rms,TOT}$ on the reef flat (Gauges 7 and 8) was over-predicted for both modes; however, significantly more so by XB-SB. This suggests that the model, with default settings, was dissipating wave energy at a slower rate than physically occurred.

Calibrating the maximum breaking wave steepness, *maxbrsteep* (Table 1) in XB-NH improved $H_{rms,TOT}$ both in the shoaling region and on the reef flat, with an average reduction in root-mean-square error, $\Delta RMSE_{Hrms,TOT}$ = 0.1 cm. Similarly, calibrating the wave dissipation coefficient, *alpha* (Table 1) in XB-SB significantly improved the $H_{rms,TOT}$ predictions on the

reef flat but at the expense of slightly under-predicting the shoaling wave height ($\Delta RMSE_{Hrms,TOT}$ = 0.1 cm). Despite this significant improvement, XB-SB still shows a minor overestimation of wave heights on the reef flat (Figure 3).

Considering the spectral wave transformation across the reef profile, XB-NH agreed well with observations at each instrument location (Figure 4). Although XB-SB does not compute the high-frequency wave spectra, it did simulate the low-frequency component of the spectra similarly well to XB-NH. In particular, the spectra over the reef flat (Figure 4g and h) are dominated by energy in the infragravity band, with peaks occurring at frequency, $f \approx 0.02$ Hz or period, $T \approx 50$ s. If we consider the reef-beach system to be an open basin with natural periods, *Tm*:

$$T_m = \frac{4l_r}{(2m-1)\sqrt{gh_r}}, m = 1, 2, 3, \ldots \quad \textbf{(19)}$$

where l_r (= 4.8 m) is the width of the reef flat, h_r = 1.6 cm (for test no. 31, Table 1) and *m* is the mode; we see that the low-frequency peaks correspond to the first reef oscillation mode (*m* = 1) at T_1 = 48.46 s. The first mode has a node at the reef crest and an anti-node at the shoreline; thus, leading to the resonant amplification of low-frequency motions at the shoreline [22,59]. This energy within the infragravity band manifests itself as long-period oscillations of the run-up signal, on top of which, short-period waves act and result in the individual run-up maxima (Figure 2).

3.3 Mean Water Level

When calibrated, there was a minor reduction of the root-mean-square error in $\bar{\eta}$ predictions for both XB-NH and XB-SB. Considering default settings, XB-NH accurately simulated setdown while $\bar{\eta}$ on the reef flat (setup)was slightly underestimated for some of the tests (Figure 5a and b). On the other hand, XB-SB underestimated wave setdown and slightly over-predicted $\bar{\eta}$ on the reef flat (Figure 5b and c). Calibration resulted in a slightly better representation of $\bar{\eta}$ over the reef flat in the XB-SB model, but had little influence on the XB-NH predictions.

3.4 Run-up

The extreme wave run-up ($R_{2\%}$ and R_{max}) model predictions, using both optimal and default parameter values, were compared to observations. The calibration improved $R_{2\%}$ predictions in both modes, but considerably more so in the XB-SB model (Figure 6). XB-NH (Figure 6b)

shows minor scatter and negligible relative bias compared to XB-SB (Figure 6d). The somewhat high positive bias shown by XB-SB even after calibration is attributed to its overestimation of wave energy on the reef flat.

With respect to R_{max}, calibration reduced scatter equally between the two XBeach modes (Figure 7). On the other hand, the relative bias was significantly reduced in XB-SB (Figure 7d) with no change to the XB-NH predictions (Figure 7b).

3.5 Calibrated Parameter Values

To assess whether the optimal values for the parameters governing wave dissipation (Table 1) may have some relationship to surfzone processes (i.e. related to key non-dimensional parameters), we consider the role of the following parameters [61,33]: i) Iribarren number, based on the fore-reef slope (ξ_0, see Equation (2)); ii) the relative reef flat submergence ($(h_r + \bar{\eta})/H_{m0}$); and iii) the offshore wave steepness ($s_0 = 2\pi H_{m0}/gT_p^2$). Optimal *maxbrsteep* parameter values show no clear dependence on any of the three parameters (Figure 8a, b and c). Similarly, optimal *alpha* parameter values show no clear relationship with Iribarren number nor offshore wave steepness (Figure 8d and f). However, there appears to be a general trend of increasing optimal *alpha* value with increased relative reef flat submergence (Figure 8e). This is in line with Yao et al. [61] who found that the water depth on the reef flat strongly affected the characteristics of wave breaking over fringing reefs and that the influence of the reef slope may be less significant.

With no clear correlation identified, the means of the optima were selected as the calibrated parameter values (*maxbrsteep* = 0.5 and *alpha* = 1.4) to be applied to the second dataset for validation (Table 1).

4 Model Validation: Application to Buckley et al. [17] Experiment

In this section the optimal parameter settings (*maxbrsteep* = 0.5 and *alpha* = 1.4) are validated on the fringing reef profile of Buckley et al. [17].

4.1 Numerical Model Setup

For XB-NH a constant grid resolution of Δx = 2.5 cm was applied; while for XB-SB, Δx was allowed to vary from 5 cm at the beach slope to 10 cm offshore. It should be noted that for the stated grid resolutions, the run time for the XB-SB simulations was on average half that of XB-NH. Both XBeach modes were forced with TMA-type spectra and initial water-levels to match

those observed offshore during the physical measurements (Table 2). The model run-time for both modes was set to 2520 s with outputs at 40 Hz at each of the 18 gauge locations to match the physical experiment.

Taking the average of the optimized parameter values previously obtained with the Demirbilek et al. [24] experiment (Section 3.5, Table 1), the XB-NH simulations were forced with *maxbrsteep* = 0.5; and the XB-SB simulations with an *alpha* = 1.4. To represent the wooden flume bottom, a Manning coefficient, $n = 0.012$ s/m$^{1/3}$ [62] was applied. Likewise, a numerical run-up gauge with *rugdepth* = 0.4 cm was specified to represent the precision of the run-up rake used during the physical experiment, which is slightly less accurate that the capacitance wire used in the previous case. This *rugdepth* value takes into account the minimum thickness of water necessary to be registered by the instrument plus the possible error due to the horizontal spacing of the rake sensors. Both XBeach modes were also run with default settings for comparison.

4.2 Wave Transformation

Compared to the model with default settings, the reduced maximum breaking wave steepness had little impact on XB-NH $H_{rms,TOT}$ predictions (Figure 9). On the other hand, the increased *alpha* value improved XB-SB $H_{rms,TOT}$ predictions on the reef flat but at the expense of further reducing $H_{rms,TOT}$ in the shoaling region. Overall XB-NH (average $RMSE_{Hrms,TOT}$ = 0.6 cm) simulated wave transformation more accurately than XB-SB (average $RMSE_{Hrms,TOT}$ = 0.9 cm) (Table 2).

Using the TMA-type boundary condition, the computed spectrum at Gauge No. 1 agrees well with observations (Figure 10a). XB-NH simulates the transformation of wave energy from the high-frequency to low-frequency bands across the reef profile and is in good agreement with observations (Figure 10). As XB-SB resolves low-frequency waves only, its exclusion of wave energy at higher frequencies is to be expected. XB-SB overpredicts the low-frequency wave energy offshore (Figure 10a); however, predictions become increasingly more accurate post wave-breaking (Figure 10e, f, g and h). Like the previous case, the reef flat is dominated by low-frequency motions (Figure 10g and h) with peaks around $f \approx 0.01$ Hz ($T \approx 100$ s). Applying Equation (19), this corresponds to the first mode based on the natural periods of the reef at T_1 = 89 s (f_1 = 0.011 Hz). Thus, infragravity motions would increase from the reef crest (Figure 10e) to the inner reef flat (Figure 10h) and shoreline.

4.3 Mean Water Levels

Compared to the model with default settings, the reduction in *maxbrsteep* had little impact on the mean water level ($\bar{\eta}$) predictions using the XB-NH model (Figure 11). What is striking, however, is the consistent under-prediction of $\bar{\eta}$ on the reef flat by XB-NH. This was observed for the majority of the 16 tests simulated but more noticeably so in those with higher H_{m0}. On the other hand, XB-SB accurately simulates $\bar{\eta}$ on the reef flat but does not quite capture setdown. The increased *alpha* value resulted in a reduction in $\bar{\eta}$ on the reef flat and a slight increase in the error compared to the model with default settings (Figure 11). Despite this, the overall error values of the XB-SB (avg. $RMSE_{MWL}$ = 0.3 cm) simulations were markedly lower than those of XB-NH (avg. $RMSE_{MWL}$ = 0.5 cm) (Table 2).

4.4 Run-up

Compared to default settings, the XB-NH and XB-SB models with the new parameter values (*maxbrsteep* = 0.5 and *alpha* = 1.4)show significant improvement in both scatter and relative bias for $R_{2\%}$ (Figure 12) and R_{max} (Figure 13) predictions. Like the previous case, this improvement is most noticeable in the XB-SB model which shows a high relative bias in its $R_{2\%}$ predictions (with default settings) (Figure 12c). Overall both modes with calibrated parameter settings show minor scatter and relative bias error values. Both XBeach modes perform comparably well despite the fact that sea-swell band motions are not explicitly computed by XB-SB and the consistent under-prediction in $\bar{\eta}$ on the reef flat observed by XB-NH.

5 Discussion

5.1 The Influence of Key Parameters Governing Wave Breaking Dissipation

The key parameters controlling the dissipation of wave energy by breaking in XB-NH (*maxbrsteep*) and XB-SB (*alpha*) were optimized for fringing reef environments using the Demirbilek et al. [24] dataset. To have confidence in the model predictions, the parameter values obtained through calibration should be physically based. In XB-NH, the onset of wave breaking is controlled by the maximum breaking wave steepness criterion and specified by the *maxbrsteep* (by default = 0.6) parameter. On the other hand, the dissipation coefficient, *alpha* (by default = 1) is a calibration constant in the wave breaking formulation and governs the rate of dissipation by breaking waves. The steep forereef slopes of fringing-reef environments are

known to cause intense dissipation of waves in a relatively narrow zone (reef crest) which then reform as bores and propagate across the reef flat before reaching the shoreline as run-up. The model must therefore correctly capture this wave attenuation to ensure the accuracy of the wave-height estimates on the reef flat. In XB-NH this was achieved by reducing *maxbrsteep* (calibrated value = 0.5) and allowing wave-breaking to initiate sooner. In XB-SB, *alpha* was increased (calibrated value = 1.4) to mimic the rapid and intense dissipation of wave energy at the reef crest.

Our results are also in line with Roelvink et al. [63] who found that reducing *maxbrsteep* to 0.4 led to an improved representation of wave-heights over a dike profile; and with Van Geer et al. [64] who recommended a higher-than-default *alpha* value of 1.26 in their systematic derivation of optimal XBeach 1D settings for application on mild-sloping sandy coasts in the Netherlands. Similarly, Su et al. [65] found optimal *alpha* values between 1.1 and 1.6 in their application of a similar dissipation model [66] to the Demirbilek et al. [24] dataset. However, the reduced *maxbrsteep* value is in contrast with Buckley et al. [33] who found much higher optimal values for the equivalent parameter in his application of the SWASH (one-layer) model to the same case [24]. Though XB-NH and SWASH (one-layer) are comparable, the models utilize slightly different criteria for the hydrostatic front approximation. Additionally, Buckley et al. [33] optimized their model considering sea-swell root-mean-square wave height ($H_{rms,SS}$) alone, whereas both the total root-mean-square wave height ($H_{rms,TOT}$) and mean water level ($\bar{\eta}$) are considered here. Therefore, the difference between results is not unexpected.

The overall impact of reducing *maxbrsteep* in XB-NH and increasing *alpha* in XB-SB were similar for both modes; that is, an improved representation of wave energy on the reef flat was observed. Use of these new parameter values also resulted in a reduction in the maximum wave-height (more so in XB-SB), a slightly earlier onset of breaking and a reduction in $\bar{\eta}$ on the reef flat (negligible in the XB-NH mode). Given that the identified parameter values are based on a 1D (alongshore uniform) fringing reef profile without large bottom roughness, further work should assess how these parameter values may change for different types of reefs in a field setting displaying different morphological and bottom roughness characteristics.

It may be argued that XB-SB, having more tuneable parameters, may be better calibrated for a particular site and range of conditions once data is available; while, XB-NH, as a more complete model may be more applicable to areas where data is limited. However, in the present study we considered only a single parameter in each model mode for calibration. Likewise,

both models were calibrated on one dataset and then applied to another for validation, with no further tuning. Thus, their performance here is considered comparable.

5.2 Wave Transformation and Mean Water Level on the Reef Flat

XB-NH with calibrated parameter values accurately simulated the transformation of waves from high to low frequencies across the reef profile (Figure 4 and Figure 10). In addition, the model was able to capture wave shoaling over the reef slope and wave breaking near the reef crest (Figure 3 and Figure 9). However, despite the accurate representation of $H_{rms,TOT}$, $\bar{\eta}$ on the reef flat was consistently under-predicted for the Buckley et al. [17] experiment (Figure 11). Moreover, increasing the maximum wave breaking steepness offered little improvement, as seen in the model results with default settings (*maxbrsteep* = 0.6). On the other hand, XB-SB with calibrated parameter values under-predicted $H_{rms,TOT}$ in the shoaling region but overestimated $H_{rms,TOT}$ on the reef flat. Unlike its short-wave resolving counterpart, XB-SB was able to quite accurately predict $\bar{\eta}$ on the reef flat which suggests that the discrepancy is specific to the XB-NH mode.

Considering previous studies, similar results using short-wave resolving wave models were obtained by Stansby and Feng [67] who also found significant under-predictions in mean water level (setup) when their non-linear shallow water wave model was compared to observations for a laboratory experiment with a steep dike profile (1:2 slope). That study found significant variation in the observed velocity, with high velocities in the upper (roller) region and almost stagnant water below. However, their depth-averaged model, like XB-NH, was unable to accurately capture these distinct zones in the water column.

With respect to reef environments, Yao et al. [68] also compared their fully non-linear Boussinesq model to the results of several laboratory fringing reef experiments. Like the present study, their model showed good agreement when applied to the Demirbilek et al. [24] dataset but also under-predicted setup on the reef flat when applied to a steeper reef profile (1:6 slope) under plunging waves. Likewise, Fang et al. [31] concluded that their Boussinesq numerical model, like several others, had a tendency to underestimate setup on the reef flat. This was especially the case for highly non-linear waves.

Collectively, these findings lend support to those of Buckley et al. [17] who found, by analysing the detailed cross-shore momentum balances through the surfzone, that excluding wave roller dynamics led to an under-prediction in mean water level on the reef flat. A wave roller,

described simply as passive areas of circulating water transported onshore by breaking waves, is considered to be one of the main contributors to nonlinear wave forcing in the surfzone [69]. Depth-averaged short-wave resolving models, based on either non-linear shallow water or Boussinesq equations, do not simulate wave overturning or plunging. Consequently, they exclude the formation and impact of wave rollers that act as an additional source of kinetic energy (KE) and result in a higher $\bar{\eta}$ on the reef flat. Thus, XB-NH may accurately predict $H_{rms,TOT}$ a measure of potential energy (PE) but under-predict the total wave energy (PE + KE). In line with the findings of Fang et al. [31], the under-prediction of wave-induced setup became more significant with increased wave nonlinearity (A_0/h) (Table 2). By disabling the roller model in XB-SB we are able to demonstrate the impact of the wave roller on setup predictions (Figure 14). XB-SB, without wave roller dynamics, also considerably underestimates $\bar{\eta}$ on the reef flat, further confirming the importance of including these dynamics in wave models applied to steep reef slopes.

5.3 Extreme Wave Run-up

When applying the model to the Buckley et al. [17] experiment, both XBeach modes showed some deviations from observations in their prediction of wave heights and mean water levels: XB-NH in its under-prediction of setup on the reef flat and XB-SB with its over-prediction of wave energy on the reef flat. Yet, both modes predicted $R_{2\%}$ (Figure 12) and R_{max} (Figure 13) with a high degree of accuracy, with only minor scatter and relative bias error values. To further investigate this, the model performance in simulating the individual physical processes that contribute to total run-up (shoreline setup and swash) was also assessed (Figure 15).

Even though XB-NH under-predicted shoreline set-up, $<\eta>$ (Rel. bias = -0.082), the overall scatter is relatively small and likely within acceptable limits (SCI $\leq$ 0.15, following Roelvink et al. [70]) (Figure 15a). Likewise, infragravity-band swash, S_{IG} is quite accurately predicted by XB-NH with almost no bias (Figure 15c). On the other hand, sea-swell band swash, S_{SS} shows relatively high scatter but minor positive relative bias (Figure 15e). It appears that the accurate representation of the dominant S_{IG} parameter coupled with the minor underestimation of $<\eta>$ and minor over-prediction of S_{SS} allowed the XB-NH model to estimate total run-up reasonably well.

From the cumulative frequency curves (Figure 16a, b and c) we see that compared to observations, the XB-NH curve is shifted to the left but with a similar steepness. This shift suggests that the mean of the XB-NH run-up time series is lower than that of the observed, as

seen also in the $<\eta>$ model-data comparison (Figure 15a). On the other hand, the similarity in shape suggests that the standard deviation of the XB-NH run-up time series is similar to what was observed, as can also be seen in the S_{IG} and S_{SS} comparisons (Figure 15c and e).

In contrast, the XB-SB cumulative frequency curves are shifted slightly to the right of that observed, suggesting that the mean of the distribution is higher than that of the observed (Figure 16a, b and c). This is also observed in the $<\eta>$ model-data comparison plot where the model shows acceptable scatter but a high positive rel. bias (Figure 15b). In line with previous studies, XB-SB predicts S_{IG} (Figure 15d) more accurately than S_{SS} (Figure 15f); with S_{SS} predictions showing substantial scatter and negative relative bias. Although more accurate, S_{IG} predictions show relatively high scatter and positive bias. This is attributed to the XB-SB model's overestimation of wave energy on the reef flat. Although not shown here, it is also worth noting that XB-SB, with the roller model turned off, considerably under-predicted total run-up and its components: $<\eta>$, S_{SS} and S_{IG}.

In line with previous studies, our results also show the presence of a trapped infragravity wave over the reef flat (Figure 4 and Figure 10) which is resonantly amplified at the shoreline [22,59]. Both the modelled and observed swash spectra confirm that the majority of the energy at the shoreline is indeed in the infragravity band (Figure 16d, e and f). This fact, along with the overestimation of $<\eta>$ compensated for the under-prediction of S_{SS} by XB-SB and allowed the short-wave averaged (but wave-group resolving) model to perform comparably well to XB-NH.

6 Conclusions

The short-wave resolving and short-wave averaged modes of the XBeach numerical model were applied to simulate wave run-up for two fringing reef profiles. To mimic the rapid and intense wave dissipation during breaking, the key parameters in each model (*maxbrsteep* in XB-NH and *alpha* in XB-SB) were calibrated on a dataset of wave breaking and run-up over a relatively steep composite slope [24]. The calibrated model was then applied to the second dataset of wave transformation and run-up over an even steeper constant slope for validation [17]. Results show good agreement with observations and suggest that in fringing reef environments XB-SB is able to perform on-par with XB-NH in predicting extreme wave run-up. This is in contrast with literature on typical, sandy coasts [47,71,72] but may be explained,

582 in part, by the dominance of infragravity motions at the shoreline; and secondly, due to the
583 exclusion of wave roller dynamics in XB-NH.

584 This study demonstrated the ability of the XBeach numerical model to accurately predict
585 extreme wave run-up. Given the limited applicability of the existing empirical models to
586 fringing reef-lined coasts, XBeach may prove to be a powerful tool for coastal flood mitigation
587 in tropical and subtropical regions. Future work should examine the effect of coral reef
588 roughness on run-up predictions by applying the model to a fringing reef with large bottom
589 roughness (e.g. Buckley et al. [73] dataset). As both experiments considered here had smooth
590 bottoms, the influence of bottom friction was not assessed. Likewise, both datasets comprised
591 one-dimensional profiles. Therefore, future work should also extend the application of XBeach
592 to field cases in 2DH to assess the influence of alongshore variability in reef morphology on
593 run-up. Finally, the incorporation of wave roller dynamics in the short-wave resolving XB-NH
594 model should be considered. Such an approach would build on work done by Madsen et al. [74]
595 who applied a geometrical approach to determine the shape, position and overall impact of the
596 wave roller on the momentum flux.

597 ## Acknowledgements

598 IHE-Delft, Institute for Water Education supported this research through the Advanced Class
599 in Translating Science to Application program. Deltares provided access to resources that was
600 fundamental to the successful completion of this research through the "Hydro- and
601 morphodynamics during extreme events" program 11200604. Ryan Lowe acknowledges
602 funding through an ARC Future Fellowship grant (FT110100201) and ARC Discovery Project
603 grant (DP140102026). Mark Buckley was funded by the USGS Mendenhall Postdoctoral
604 Fellowship Program and the USGS Coastal and Marine Geology Program. The authors would
605 also like to acknowledge Dr. Zeki Demirbilek, Dr. Okey Nwogu and Dr. Donald L. Ward for
606 the published data used in this study.

References

[1] Holman, R.A. and Sallenger, A.H., 1985. *Setup and swash on a natural beach. Journal of Geophysical Research: Oceans*, 90(C1): 945-953.

[2] Stockdon, H.F., Holman, R.A., Howd, P.A. and Sallenger, A.H., 2006. *Empirical parameterization of setup, swash, and runup. Coastal Engineering*, 53(7): 573-588.

[3] Didier, D., Bernatchez, P., Marie, G. and Boucher-Brossard, G., 2016. *Wave runup estimations on platform-beaches for coastal flood hazard assessment. Natural Hazards*, 83(3): 1443-1467.

[4] Gallien, T., 2016. *Validated coastal flood modeling at imperial beach, california: Comparing total water level, empirical and numerical overtopping methodologies. Coastal Engineering*, 111: 95-104.

[5] Massel, S.R. and Gourlay, M.R., 2000. *On the modelling of wave breaking and set-up on coral reefs. Coastal Engineering*, 39(1): 1-27.

[6] Sallenger, A.H., 2000. *Storm impact scale for barrier islands. Journal of Coastal Research*, 16(3): 890-895.

[7] Cheriton, O.M., Storlazzi, C.D. and Rosenberger, K.J., 2016. *Observations of wave transformation over a fringing coral reef and the importance of low-frequency waves and offshore water levels to runup, overwash, and coastal flooding. Journal of Geophysical Research: Oceans*, 121(5): 3121-3140.

[8] Wang, Y.-H., Lee, I.H. and Wang, D.-P., 2005. *Typhoon induced extreme coastal surge: A case study at northeast taiwan in 1994. Journal of Coastal Research*: 548-552.

[9] Wolf, J., 2009. *Coastal flooding: Impacts of coupled wave–surge–tide models. Natural Hazards*, 49(2): 241-260.

[10] Holman, R.A., 1986. *Extreme value statistics for wave run-up on a natural beach. Coastal Engineering*, 9(6): 527-544.

[11] Nielsen, P. and Hanslow, D., 1991. *Wave runup distributions on natural beaches. Journal of Coastal Research*, 7(4): 1139-1152.

[12] Hedges, T.S. and Mase, H., 2004. *Modified hunt's equation incorporating wave setup. Journal of Waterway, Port, Coastal, and Ocean Engineering*, 130(3): 109-113.

[13] Munk, W.H. and Sargent, M.C., 1948. *Adjustment of bikini atoll to ocean waves. Eos, Transactions American Geophysical Union*, 29(6): 855-860.

[14] Gerritsen, F., 1980. Wave attenuation and wave set-up on a coastal reef, Coastal engineering 1980, pp. 444-461.

[15] Kench, P.S. and Brander, R.W., 2006. *Wave processes on coral reef flats: Implications for reef geomorphology using australian case studies. Journal of Coastal Research*: 209-223.

[16] Lowe, R.J., Falter, J.L., Monismith, S.G. and Atkinson, M.J., 2009. *Wave-driven circulation of a coastal reef–lagoon system. Journal of Physical Oceanography*, 39(4): 873-893.

[17] Buckley, M.L., Lowe, R.J., Hansen, J.E. and Van Dongeren, A.R., 2015. *Dynamics of wave setup over a steeply sloping fringing reef. Journal of Physical Oceanography*, 45(12): 3005-3023.

[18] Pomeroy, A., Lowe, R., Symonds, G., Van Dongeren, A. and Moore, C., 2012. *The dynamics of infragravity wave transformation over a fringing reef. Journal of Geophysical Research: Oceans*, 117(C11).

[19] Péquignet, A.-C.N., Becker, J.M. and Merrifield, M.A., 2014. *Energy transfer between wind waves and low-frequency oscillations on a fringing reef, ipan, guam. Journal of Geophysical Research: Oceans*, 119(10): 6709-6724.

[20] van Dongeren, A., de Jong, M., van der Lem, C., van Deyzen, A. and den Bieman, J., 2016. *Review of long wave dynamics over reefs and into ports with implication for port operations. Journal of Marine Science and Engineering*, 4(1): 12.
[21] Lowe, R.J. et al., 2005. *Spectral wave dissipation over a barrier reef. Journal of Geophysical Research: Oceans*, 110(C4): n/a-n/a.
[22] Nwogu, O. and Demirbilek, Z., 2010. *Infragravity wave motions and runup over shallow fringing reefs. J Waterw Port C-Asce*, 136(6): 295-305.
[23] Nakaza, E. and Hino, M., 1991. *Bore-like surf beat in a reef zone caused by wave groups of incident short period waves. Fluid Dynamics Research*, 7(2): 89-100.
[24] Demirbilek, Z., Nwogu, O.G. and Ward, D.L., 2007. Laboratory study of wind effect on runup over fringing reefs. Report 1. Data report, DTIC Document.
[25] Péquignet, A.C.N., Becker, J.M., Merrifield, M.A. and Aucan, J., 2009. *Forcing of resonant modes on a fringing reef during tropical storm man-yi. Geophysical Research Letters*, 36(3): n/a-n/a.
[26] Shimozono, T. et al., 2015. *Combined infragravity wave and sea‐swell runup over fringing reefs by super typhoon haiyan. Journal of Geophysical Research: Oceans*, 120(6): 4463-4486.
[27] Sheremet, A., Kaihatu, J.M., Su, S.F., Smith, E.R. and Smith, J.M., 2011. *Modeling of nonlinear wave propagation over fringing reefs. Coastal Engineering*, 58(12): 1125-1137.
[28] Filipot, J.-F. and Cheung, K.F., 2012. *Spectral wave modeling in fringing reef environments. Coastal Engineering*, 67: 67-79.
[29] McCabe, M.V., Stansby, P.K. and Apsley, D.D., 2013. *Random wave runup and overtopping a steep sea wall: Shallow-water and boussinesq modelling with generalised breaking and wall impact algorithms validated against laboratory and field measurements. Coastal Engineering*, 74: 33-49.
[30] Van Dongeren, A. et al., 2013. *Numerical modeling of low-frequency wave dynamics over a fringing coral reef. Coastal Engineering*, 73: 178-190.
[31] Fang, K.-z., Yin, J.-w., Liu, Z.-b., Sun, J.-w. and Zou, Z.-l., 2014. *Revisiting study on boussinesq modeling of wave transformation over various reef profiles. Water Science and Engineering*, 7(3): 306-318.
[32] Ma, G., Su, S.-F., Liu, S. and Chu, J.-C., 2014. *Numerical simulation of infragravity waves in fringing reefs using a shock-capturing non-hydrostatic model. Ocean Engineering*, 85: 54-64.
[33] Buckley, M., Lowe, R. and Hansen, J., 2014. *Evaluation of nearshore wave models in steep reef environments. Ocean Dynamics*, 64(6): 847-862.
[34] Berkhoff, J., 1973. Computation of combined refraction—diffraction, Coastal engineering 1972, pp. 471-490.
[35] Booij, N., 1983. *A note on the accuracy of the mild-slope equation. Coastal Engineering*, 7(3): 191-203.
[36] Kirby, J.T. and Dalrymple, R.A., 1983. *Propagation of obliquely incident water waves over a trench. Journal of Fluid Mechanics*, 133: 47-63.
[37] Roelvink, D. et al., 2009. *Modelling storm impacts on beaches, dunes and barrier islands. Coastal Engineering*, 56(11-12): 1133-1152.
[38] Harley, M., Armaroli, C. and Ciavola, P., 2011. *Evaluation of xbeach predictions for a real-time warning system in emilia-romagna, northern italy. Journal of Coastal Research*(64): 1861.
[39] Cox, N., Dunkin, L.M. and Irish, J.L., 2013. *An empirical model for infragravity swash on barred beaches. Coastal Engineering*, 81: 44-50.

[40] Masselink, G., McCall, R., Poate, T. and Geer, P.v., 2014. *Modelling storm response on gravel beaches using xbeach-g. Proceedings of the Institution of Civil Engineers - Maritime Engineering*, 167(4): 173-191.
[41] McCall, R.T., Masselink, G., Poate, T.G., Roelvink, J.A. and Almeida, L.P., 2015. *Modelling the morphodynamics of gravel beaches during storms with xbeach-g. Coastal Engineering*, 103: 52-66.
[42] Quataert, E., Storlazzi, C., van Rooijen, A., Cheriton, O. and van Dongeren, A., 2015. *The influence of coral reefs and climate change on wave-driven flooding of tropical coastlines. Geophysical Research Letters*.
[43] Storlazzi, C., Quataert, E. and Pearson, S., 2017. Wave dynamics and flooding on low-lying tropical reef-lined coasts. *Coastal Dynamics 2017*, p.^pp. 654-664.
[44] Pearson, S.G., Storlazzi, C.D., van Dongeren, A.R., Tissier, M.F.S. and Reniers, A.J.H.M., 2017. *A bayesian-based system to assess wave-driven flooding hazards on coral reef-lined coasts. Journal of Geophysical Research: Oceans*, 122(12): 10099-10117.
[45] Raichlen, F. and Hammack Jr, J., 1975. Run-up due to breaking and non-breaking waves, Coastal engineering 1974, pp. 1937-1955.
[46] Gent, M.R.A.v., 2001. *Wave runup on dikes with shallow foreshores. Journal of Waterway, Port, Coastal, and Ocean Engineering*, 127(5): 254-262.
[47] Stockdon, H.F., Thompson, D.M., Plant, N.G. and Long, J.W., 2014. *Evaluation of wave runup predictions from numerical and parametric models. Coastal Engineering*, 92: 1-11.
[48] Zijlema, M., Stelling, G. and Smit, P., 2011. *Swash: An operational public domain code for simulating wave fields and rapidly varied flows in coastal waters. Coastal Engineering*, 58(10): 992-1012.
[49] Smagorinsky, J., 1963. *General circulation experiments with the primitive equations. Monthly Weather Review*, 91(3): 99-164.
[50] Smit, P. et al., 2010. *Xbeach: Non-hydrostatic model: Validation, verification and model description. Delft University of Technology*.
[51] Smit, P., Zijlema, M. and Stelling, G., 2013. *Depth-induced wave breaking in a non-hydrostatic, near-shore wave model. Coastal Engineering*, 76: 1-16.
[52] Holthuijsen, L.H., Booij, N. and Herbers, T.H.C., 1989. *A prediction model for stationary, short-crested waves in shallow water with ambient currents. Coastal Engineering*, 13(1): 23-54.
[53] Roelvink, J.A., 1993. *Dissipation in random wave groups incident on a beach. Coastal Engineering*, 19(1): 127-150.
[54] Svendsen, I.A., 1984. *Wave heights and set-up in a surf zone. Coastal Engineering*, 8(4): 303-329.
[55] Nairn, R.B., Roelvink, J. and Southgate, H.N., 1991. Transition zone width and implications for modelling surfzone hydrodynamics, Coastal engineering 1990, pp. 68-81.
[56] Holthuijsen, L.H., 2007. *Waves in oceanic and coastal waters*.
[57] Roelvink, J.A. and Stive, M.J.F., 1989. *Bar‐generating cross‐shore flow mechanisms on a beach. Journal of Geophysical Research: Oceans (1978–2012)*, 94(C4): 4785-4800.
[58] Douglas, S.L., 1990. Estimating runup on beaches: A review of the state of the art, UNIVERSITY OF SOUTH ALABAMA MOBILE.
[59] Zijlema, M., 2012. Modelling wave transformation across a fringing reef using swash. *ICCE 2012: Proceedings of the 33rd International Conference on Coastal Engineering, Santander, Spain, 1-6 July 2012*, p.^pp.

[60] Roelvink, D. et al., 2015. *Xbeach technical reference: Kingsday release. Delft, The Netherlands: Deltares, Technical report*.
[61] Yao, Y., Huang, Z., Monismith, S.G. and Lo, E.Y.M., 2013. *Characteristics of monochromatic waves breaking over fringing reefs. Journal of Coastal Research*: 94-104.
[62] Chow, V.T., 1959. *Open channel flow. London: McGRAW-HILL*, 11(95): 99,136-140.
[63] Roelvink, D. et al., 2015. Risc-kit: Improvement of physical processes xbeach improvement & validation; wave dissipation over vegetated marshes and flash flood module.
[64] Van Geer, P., den Bieman, J., Hoonhout, B. and Boers, M., 2015. *Xbeach 1d-probabilistic model. Adis, settings, model uncertainty and graphical user interface. Tec. Rep*: 1209436-002.
[65] Su, S.-F., Sheremet, A. and Smith, J.M., 2011. *Parametric wave-breaking on steep reefs. 2011*(32).
[66] Janssen, T.T. and Battjes, J.A., 2007. *A note on wave energy dissipation over steep beaches. Coastal Engineering*, 54(9): 711-716.
[67] Stansby, P.K. and Feng, T., 2004. *Surf zone wave overtopping a trapezoidal structure: 1-d modelling and piv comparison. Coastal Engineering*, 51(5): 483-500.
[68] Yao, Y., Huang, Z., Monismith, S.G. and Lo, E.Y., 2012. *1dh boussinesq modeling of wave transformation over fringing reefs. Ocean Engineering*, 47: 30-42.
[69] Apotsos, A., Raubenheimer, B., Elgar, S., Guza, R.T. and Smith, J.A., 2007. *Effects of wave rollers and bottom stress on wave setup. Journal of Geophysical Research: Oceans*, 112(C2): n/a-n/a.
[70] Roelvink, D., McCall, R., Mehvar, S., Nederhoff, K. and Dastgheib, A., 2017. *Improving predictions of swash dynamics in xbeach: The role of groupiness and incident-band runup. Coastal Engineering*.
[71] Quataert, E., 2015. Wave runup on atoll reefs. MSc. Thesis, TU Delft.
[72] Palmsten, M.L. and Splinter, K.D., 2016. *Observations and simulations of wave runup during a laboratory dune erosion experiment. Coastal Engineering*, 115: 58-66.
[73] Buckley, M.L., Lowe, R.J., Hansen, J.E. and Dongeren, A.R.V., 2016. *Wave setup over a fringing reef with large bottom roughness. Journal of Physical Oceanography*, 46(8): 2317-2333.
[74] Madsen, P.A., Sørensen, O.R. and Schäffer, H.A., 1997. *Surf zone dynamics simulated by a boussinesq type model. Part i. Model description and cross-shore motion of regular waves. Coastal Engineering*, 32(4): 255-287.

Table 1 Summary of test conditions (Demirbilek et al. [24] experiment) with Iribarren number (ξ_0) based on the forereef slope (1:10.6), relative reef flat submergence ($(h_r + \bar{\eta})/H_{m0}$), offshore wave steepness (s_0), optimal *maxbrsteep* and *alpha* values and the reduction in error ($\Delta RMSE_{TOT}$) achieved through calibration.

Test No.	H_{m0} (cm)	T_p (s)	h_r (cm)	ξ_0	$\frac{hr+\bar{\eta}}{H_{m0}}$	s_0	XB-NH		XB-SB	
							Opt. *maxbrsteep*	$\Delta RMSE_{TOT}$ (cm)	Opt. *alpha*	$\Delta RMSE_{TOT}$ (cm)
15	6.2	1	5.1	0.47	0.90	0.04	0.45	0.00	2	0.07
16	5.2	1.5	5.1	0.78	1.08	0.01	0.35	0.11	2	0.14
17	7.8	1.5	5.1	0.63	0.76	0.02	0.4	0.14	1.4	0.09
18	8.5	2	5.1	0.81	0.73	0.01	0.5	0.02	1.4	0.19
19	8.3	2.5	5.1	1.02	0.76	0.01	0.8	0.07	1.4	0.21
20	6.1	1.25	5.1	0.60	0.92	0.03	0.4	0.08	1.8	0.06
21	8.2	1.75	5.1	0.72	0.73	0.02	0.4	0.11	1.4	0.13
26	5.8	1	1.6	0.49	0.41	0.04	0.8	0.02	1.25	0.04
27	5.5	1.25	1.6	0.63	0.47	0.02	0.75	0.02	1.35	0.08
28	4.7	1.5	1.6	0.82	0.55	0.01	0.3	0.02	1.75	0.17
29	7.1	1.5	1.6	0.66	0.42	0.02	0.3	0.07	1.2	0.07
30	7.6	1.75	1.6	0.75	0.42	0.02	0.35	0.16	1.35	0.19
31	8.5	2	1.6	0.81	0.41	0.01	0.45	0.09	1.35	0.24
32	7.9	2.5	1.6	1.05	0.46	0.01	0.7	0.04	1.35	0.23
33	5.6	1	0	0.50	0.20	0.04	0.8	0.03	1.15	0.02
34	4.5	1.5	0	0.83	0.27	0.01	0.3	0.06	1.4	0.16
35	4.5	1.5	0	0.83	0.29	0.01	0.35	0.05	1.4	0.16
36	6.8	1.5	0	0.68	0.26	0.02	0.35	0.08	1.1	0.05
37	7.6	1.75	0	0.75	0.26	0.02	0.35	0.31	1.2	0.15
38	8.4	2	0	0.81	0.26	0.01	0.4	0.22	1.4	0.32
39	7.7	2.5	0	1.06	0.31	0.01	0.7	0.01	1.4	0.30
44	3.2	1	3.1	0.66	1.03	0.02	0.8	0.00	1.65	0.02
45	6.1	1	3.1	0.48	0.59	0.04	0.8	0.02	1.1	0.01
46	5.9	1.25	3.1	0.61	0.63	0.02	0.8	0.01	1.35	0.06
47	5	1.5	3.1	0.79	0.74	0.01	0.35	0.01	1.65	0.12
48	7.5	1.5	3.1	0.65	0.53	0.02	0.4	0.02	1.35	0.07
57	7.7	1.75	3.1	0.74	0.55	0.02	0.35	0.08	1.25	0.11
58	8.5	2	3.1	0.81	0.52	0.01	0.45	0.05	1.3	0.19
59	8.2	2.5	3.1	1.03	0.55	0.01	0.7	0.02	1.4	0.26
Average (avg.)							0.51	0.07	1.42	0.13

Table 2 Summary of test conditions (Buckley et al. [17] experiment), Iribarren number (ξ_0) based on the forereef slope (1:5), wave nonlinearity (A_0/h) and error values in root-mean-square wave height ($RMSE_{Hrms,TOT}$) and mean water-level ($RMSE_{MWL}$) predictions. Note: A_0 = offshore wave amplitude ($H_{m0}/2$) and h = offshore water depth.

Test No.	H_{m0} (cm)	T_p (s)	h_r (cm)	ξ_0	A_0/h	XB-NH			XB-SB		
						$RMSE_{Hrms,TOT}$ (cm)	$RMSE_{MWL}$ (cm)	$RMSE_{TOT}$ (cm)	$RMSE_{Hrms,TOT}$ (cm)	$RMSE_{MWL}$ (cm)	$RMSE_{TOT}$ (cm)
1	4	2.26	4	2.82	0.03	0.27	0.05	0.32	0.49	0.06	0.55
2	8	2.26	4	2.00	0.05	0.47	0.27	0.74	0.80	0.17	0.97
3	12	2.26	4	1.63	0.08	0.57	0.47	1.04	0.90	0.36	1.26
4	16	2.26	4	1.41	0.11	0.72	0.63	1.35	1.00	0.38	1.38
5	20	2.26	4	1.26	0.14	0.60	0.86	1.46	0.97	0.48	1.45
6	24	2.26	4	1.15	0.16	0.61	1.10	1.71	1.10	0.54	1.64
7	8	1.31	4	1.16	0.05	0.69	0.40	1.09	0.64	0.24	0.88
8	8	3.2	4	2.83	0.05	0.64	0.34	0.98	1.10	0.31	1.41
9	8	2.26	0	2.00	0.06	0.41	0.55	0.96	0.63	0.29	0.92
10	8	2.26	2	2.00	0.06	0.46	0.41	0.87	0.63	0.27	0.90
11	8	2.26	6	2.00	0.05	0.57	0.17	0.74	0.80	0.18	0.98
12	8	2.26	9	2.00	0.05	0.66	0.11	0.77	0.85	0.12	0.97
13	16	2.26	0	1.41	0.11	0.50	0.85	1.35	0.76	0.41	1.17
14	16	2.26	2	1.41	0.11	0.52	0.78	1.30	0.78	0.41	1.19
15	16	2.26	6	1.41	0.11	0.77	0.60	1.37	1.10	0.45	1.55
16	16	2.26	9	1.41	0.10	0.94	0.41	1.35	1.30	0.41	1.71
Average (avg.)						0.59	0.50	1.09	0.87	0.32	1.18

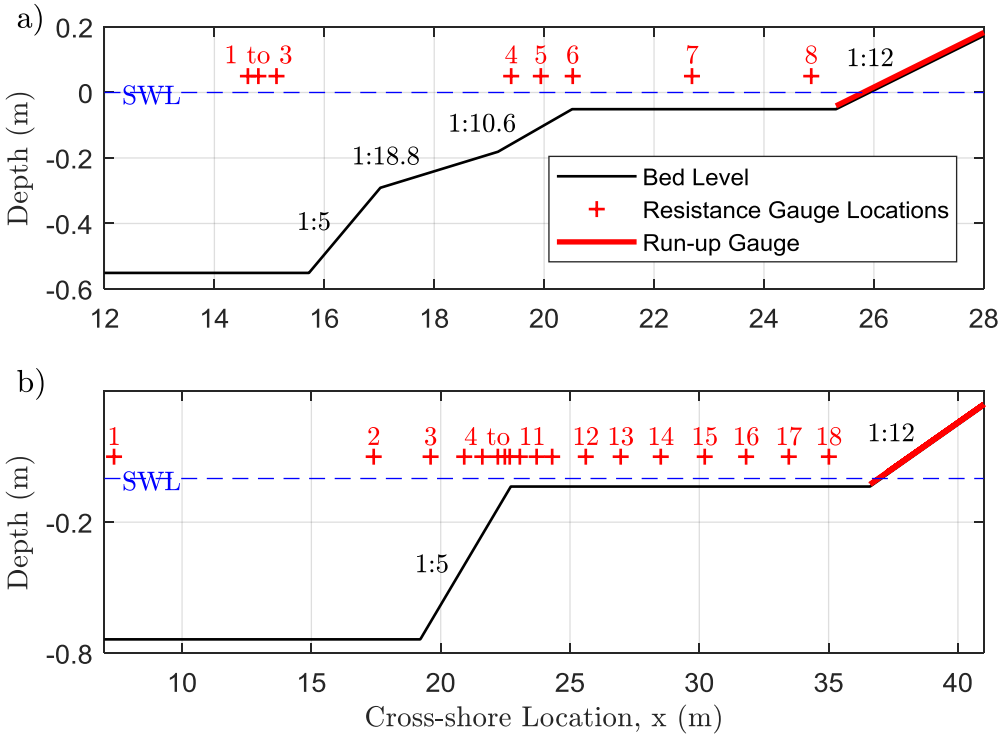

Figure 1 Profiles of fringing reefs simulated, showing instrument locations for (a) Demirbilek et al. [24] and (b) Buckley et al. [17] experiments.

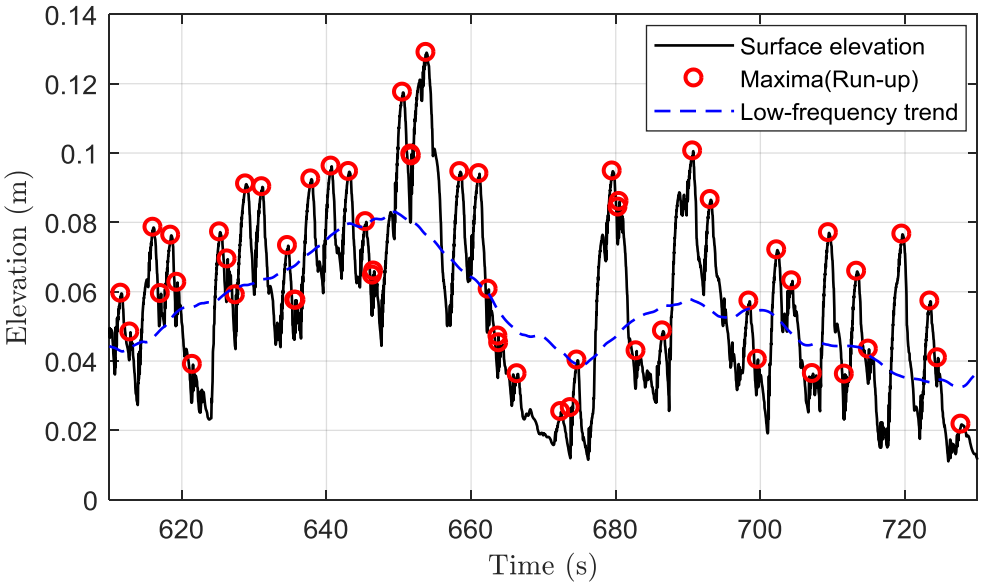

892

893 **Figure 2 Example run-up (swash)time series showing extracted maxima and low-frequency trend.**

894

895

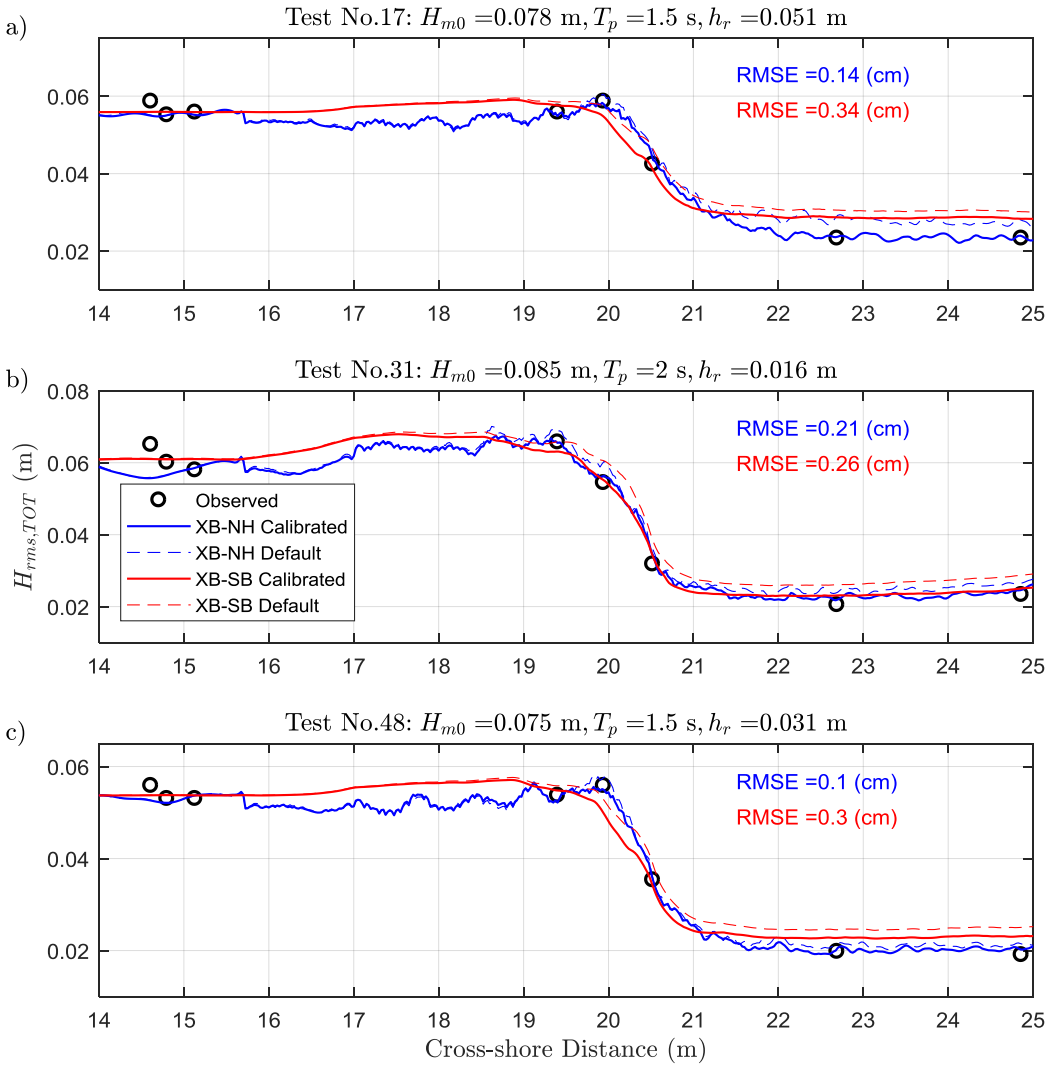

Figure 3 Modelled and observed total root-mean-square wave height ($H_{rms,TOT}$) profiles for representative tests no. (a) 17, (b) 31 and (c) 48 (Demirbilek et al. [24] experiment) for XB-NH (blue) and XB-SB (red) before (dashed lines) and after (solid lines) calibration showing root-mean-square error (RMSE) values for the calibrated runs. Note: tests were selected to cover the range of offshore wave and water level conditions simulated.

903

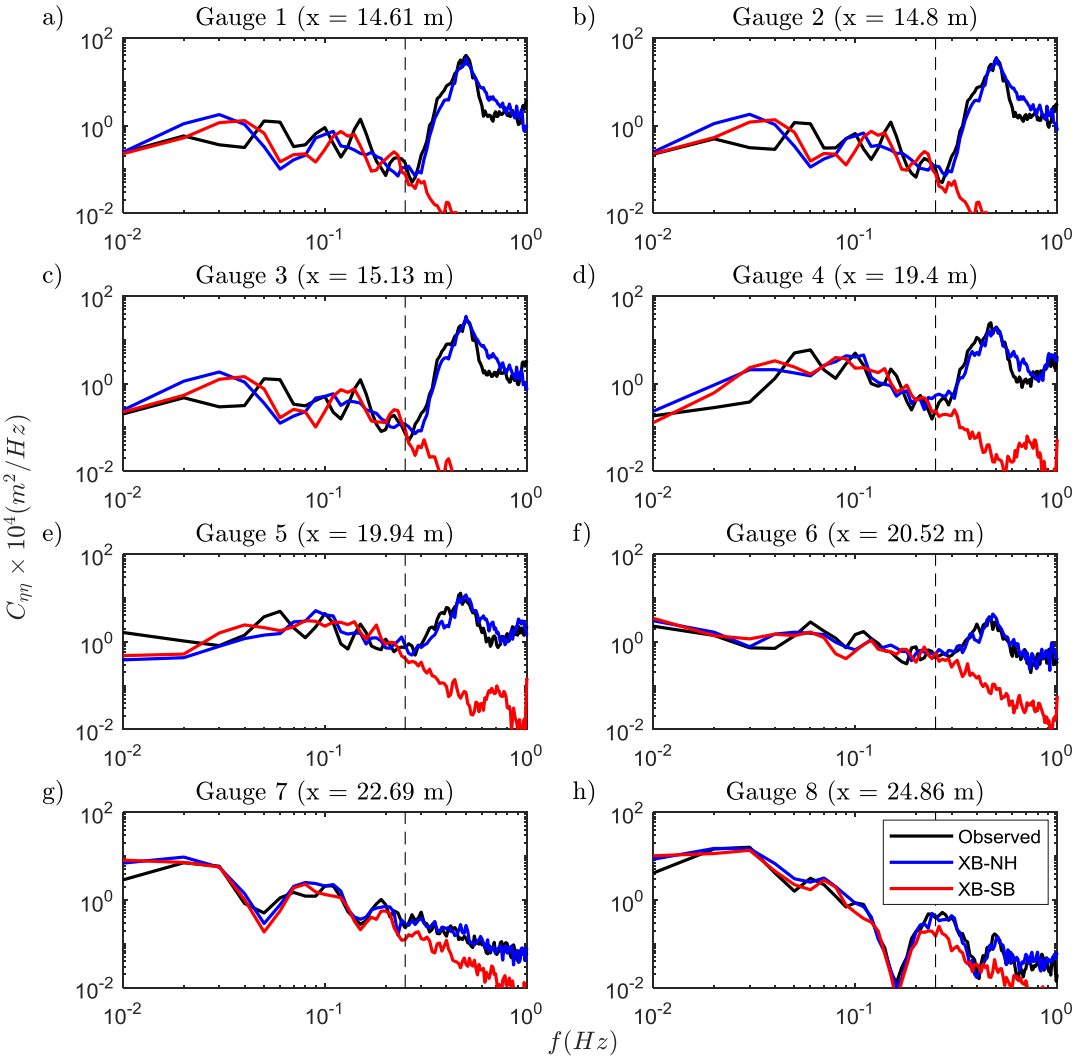

904

905 **Figure 4 Modelled and observed spectral transformation of wave energy from (a, b) offshore, (c)**
906 **the shoaling region, (d, e, f) during breaking and (g, h) on the reef flat for representative test no.**
907 **31 (Demirbilek et al. [24] experiment) for XB-NH (blue) and XB-SB (red). Dashed black lines**
908 **represent the split frequency ($f_{split} = fp/2$) and the resolution of the spectra is 0.01 Hz with**
909 **approximately 51 degrees-of-freedom.**

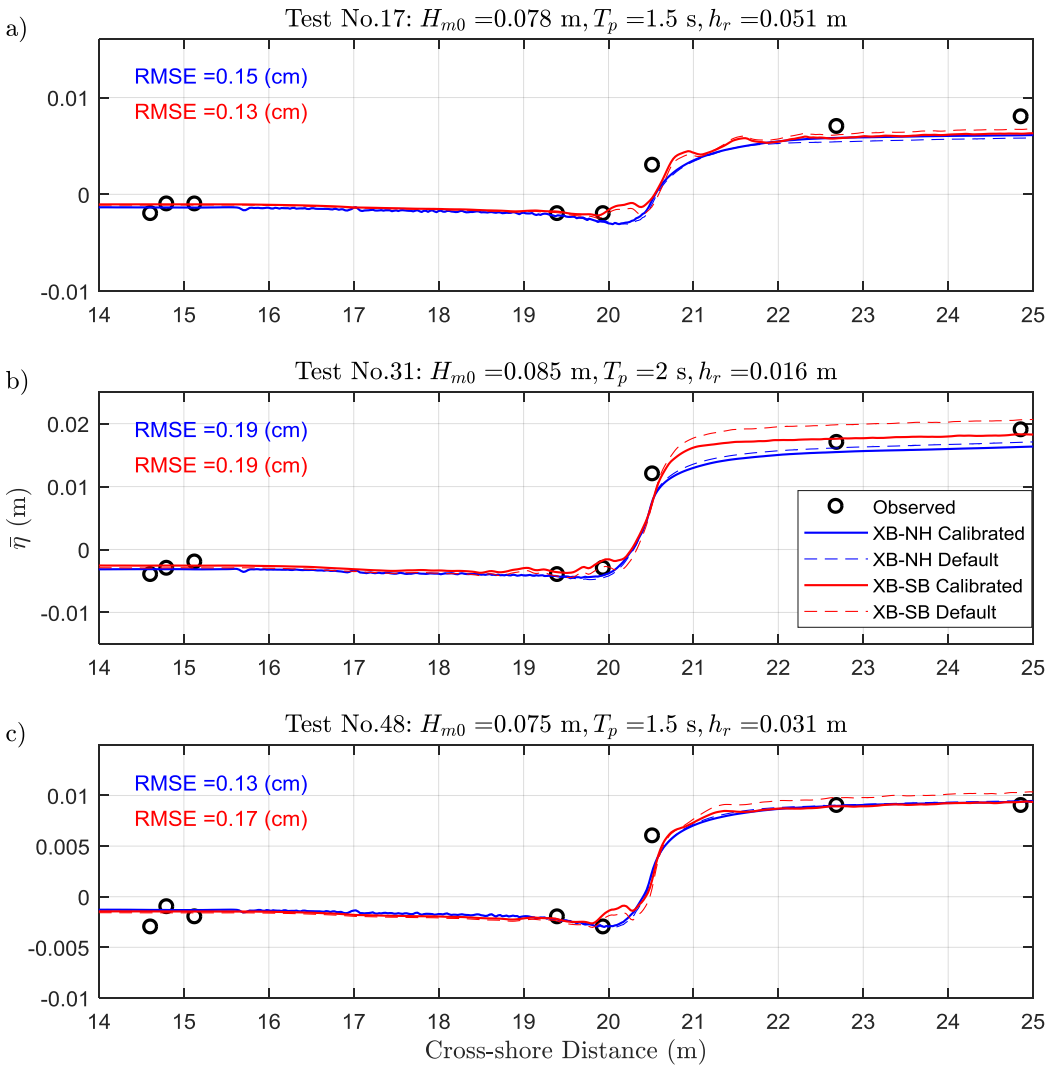

Figure 5 Modelled and observed mean water level ($\bar{\eta}$) profiles for representative tests no. (a) 17, (b) 31 and (c) 48 (Demirbilek et al. [24] experiment) for XB-NH (blue) and XB-SB (red) before (dashed lines) and after (solid lines) calibration showing root-mean-square error (RMSE) values for the calibrated runs. Note: tests were selected to cover the range of offshore wave and water level conditions simulated.

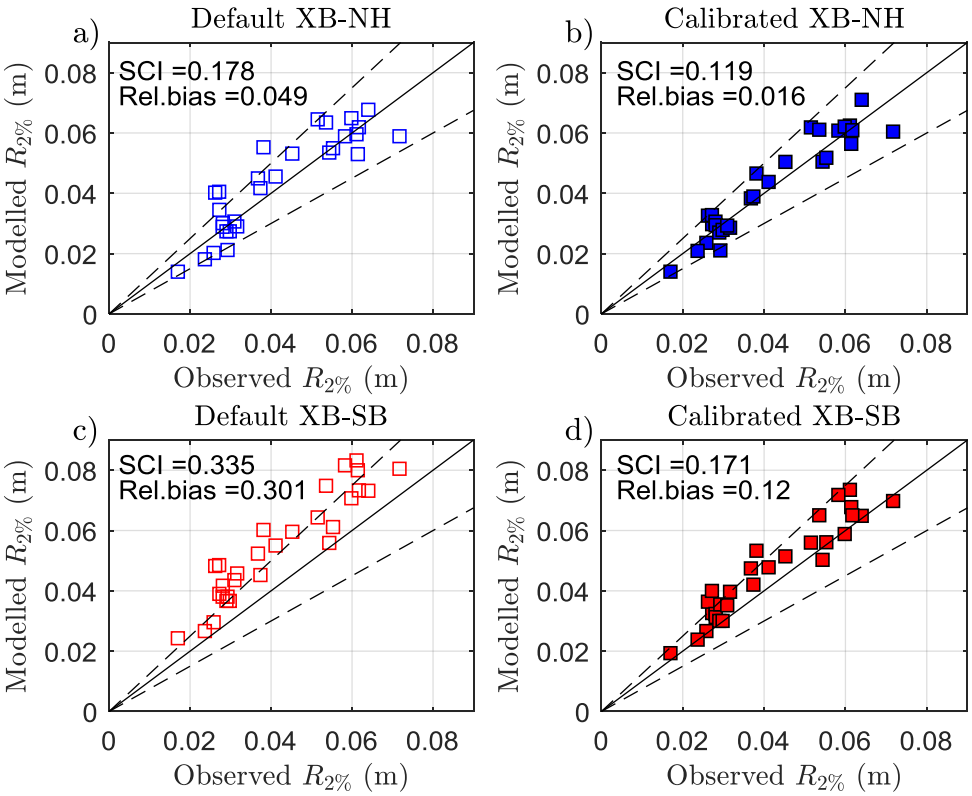

Figure 6 Modelled and observed two-percent exceedance run-up ($R_{2\%}$) comparison for XB-NH (blue) and XB-SB (red) before (unfilled) and after (filled) calibration showing SCI and Relative Bias error values (Demirbilek et al. [24] experiment). Black solid lines represent perfect agreement. Black dashed lines represent +/− 25% error.

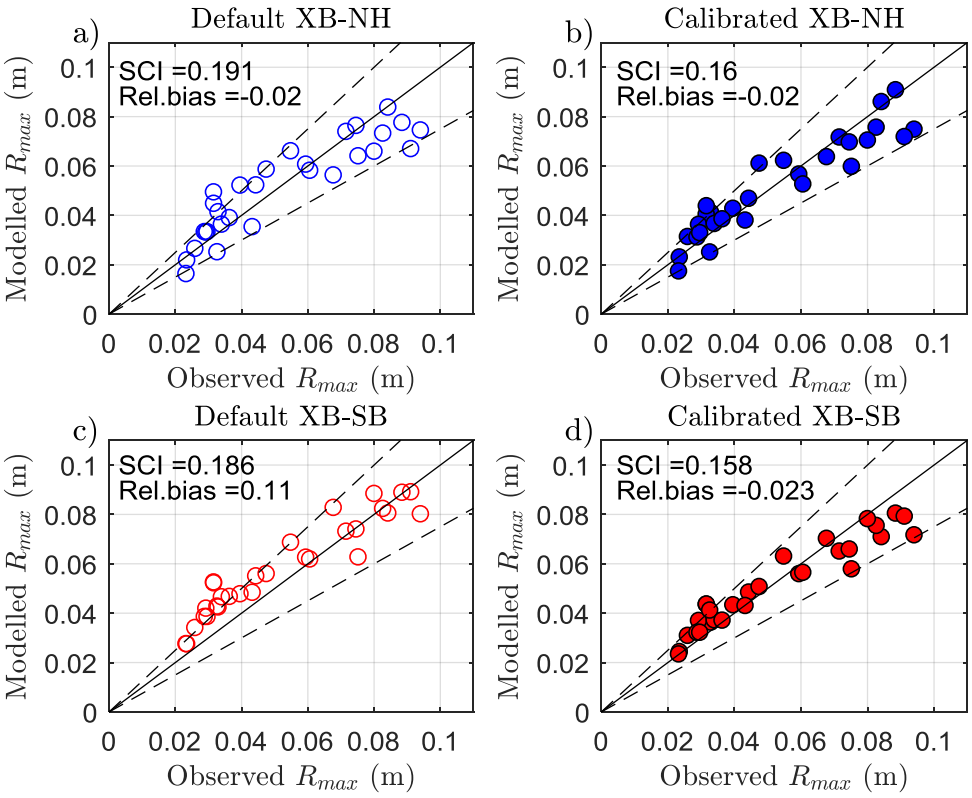

923

924 **Figure 7 Modelled and observed maximum run-up (R_{max}) comparison for XB-NH (blue) and XB-**
925 **SB (red) before (unfilled) and after (filled) calibration showing SCI and Relative Bias error values**
926 **(Demirbilek et al. [24] experiment). Black solid lines represent perfect agreement. Black dashed**
927 **lines represent +/− 25% error.**

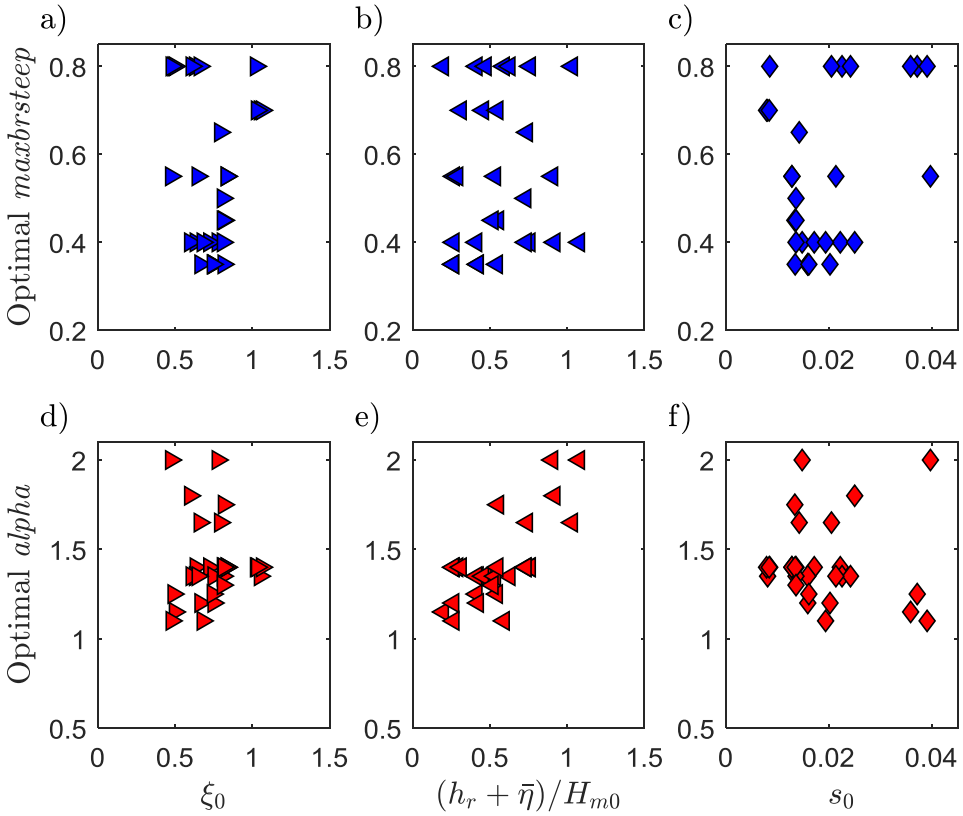

928

929 **Figure 8 Optimal *maxbrsteep* in XB-NH (blue) and *alpha* in XB-SB (red) parameter values are**
930 **compared with non-dimensional wave parameters: ξ_0 (a, d), $(h_r + \bar{\eta})/H_{m0}$ (b, e) and s_0 (c, f).**

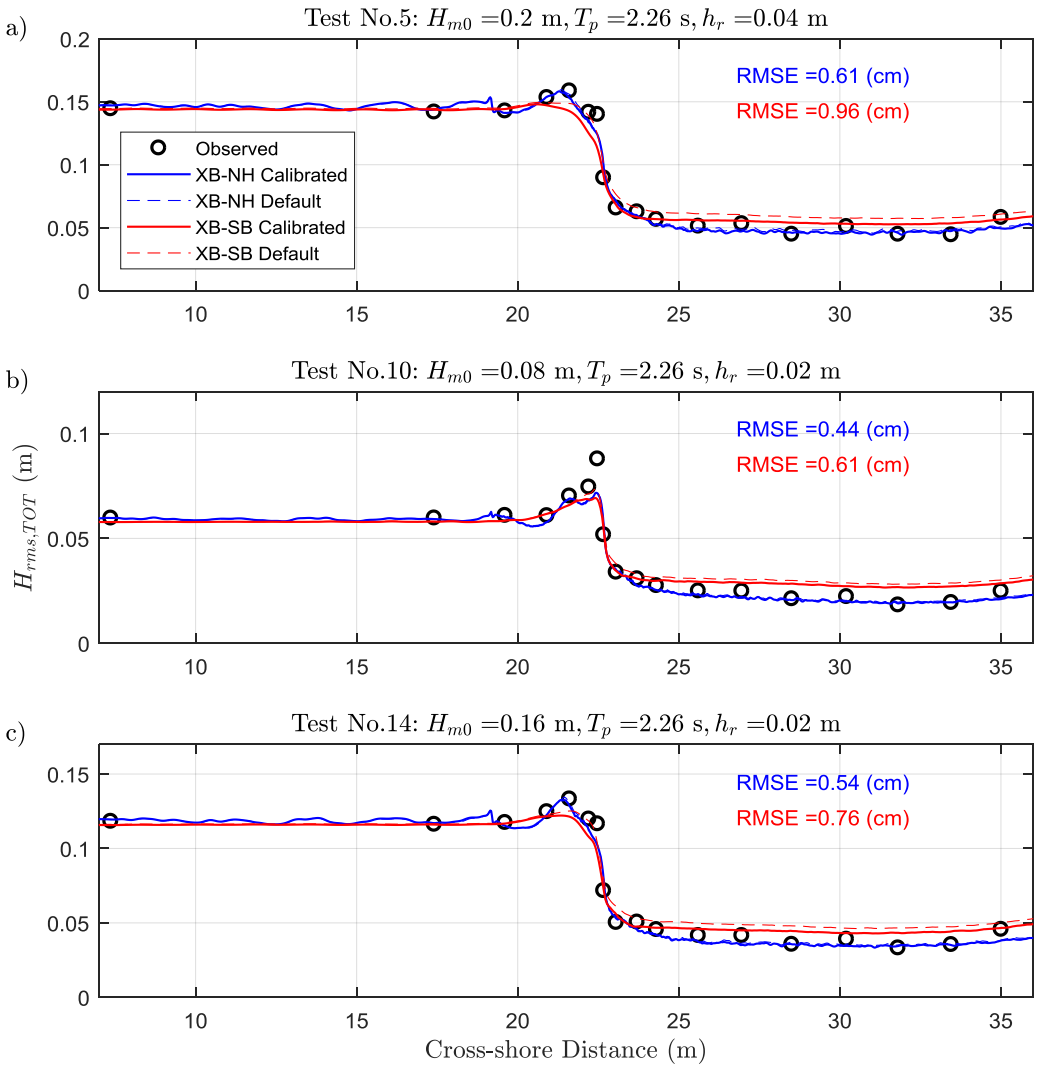

931

932 **Figure 9 Modelled and observed total root-mean-square wave height ($H_{rms,TOT}$) profiles for**
933 **representative tests no. (a) 5, (b) 10 and (c) 14 (Buckley et al. [17] experiment) for XB-NH (blue)**
934 **and XB-SB (red) with default (*maxbrsteep = 0.6, alpha = 1*) and calibrated (*maxbrsteep = 0.5, alpha*)**
935 **= *1.4*) parameter values (solid lines) showing root-mean-square error (RMSE) values. Note: tests**
936 **were selected to cover the range of offshore wave conditions simulated.**

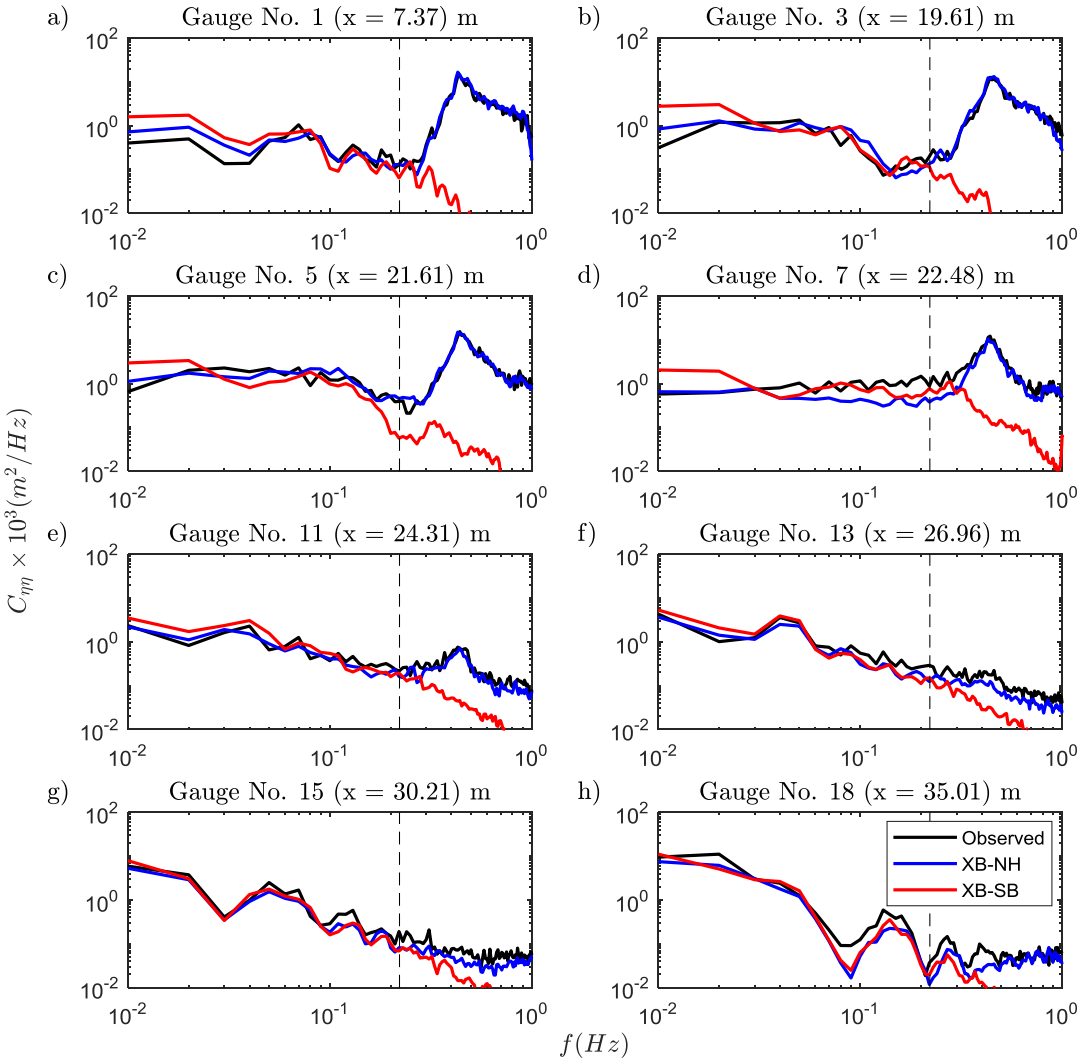

Figure 10 Modelled and observed spectral transformation of wave energy from (a, b) offshore, (c) the shoaling region, (d, e) during breaking and (f, g, h) on the reef flat for representative test no. 5 (Buckley et al. [17] experiment) for XB-NH (blue) and XB-SB (red). Dashed black lines represent the split frequency ($f_{split} = fp/2$) and the resolution of the spectra is 0.01 Hz with approximately 125 degrees-of-freedom.

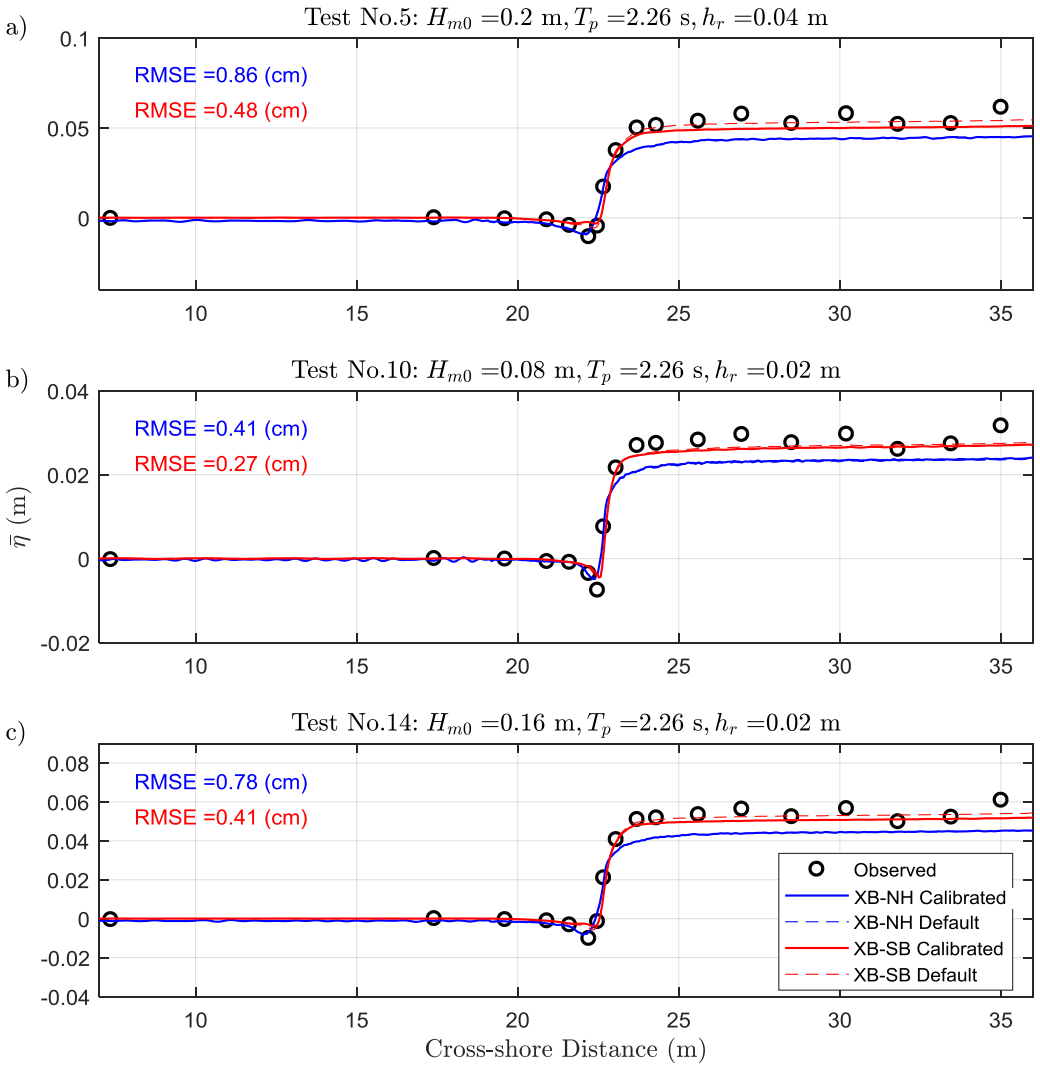

Figure 11 Modelled and observed mean water level ($\overline{\eta}$) profiles for representative tests no. (a) 5, (b) 10 and (c) 14 (Buckley et al. [17] experiment) for XB-NH (blue) and XB-SB (red) with default (*maxbrsteep = 0.6, alpha = 1*) and calibrated (*maxbrsteep = 0.5, alpha = 1.4*) parameter values showing root-mean-square error (RMSE) values. Note: tests were selected to cover the range of offshore wave conditions simulated.

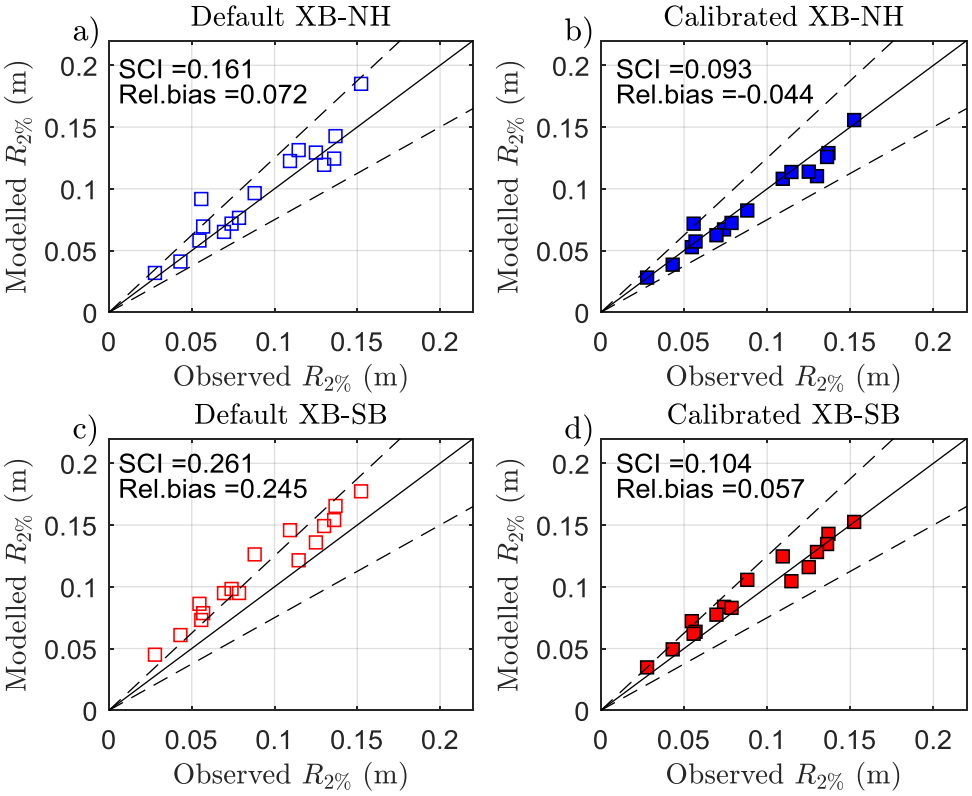

952

953 **Figure 12 Modelled and observed two-percent exceedance run-up ($R_{2\%}$) comparison for XB-NH**
954 **(blue) and XB-SB (red) with default (*maxbrsteep = 0.6, alpha = 1*) and calibrated (*maxbrsteep =***
955 ***0.5, alpha = 1.4*) parameter values showing SCI and Relative Bias error values (Buckley et al. [17]**
956 **experiment). Black solid lines represent perfect agreement. Black dashed lines represent $+/-$ 25%**
957 **error.**

958

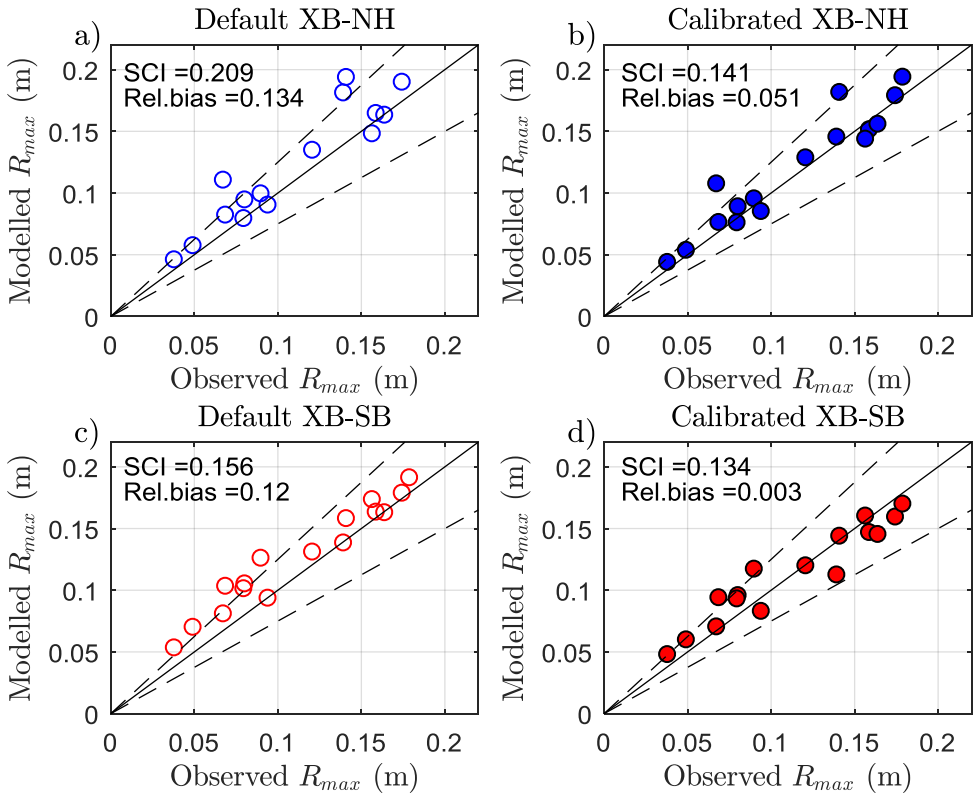

959

960 **Figure 13 Modelled and observed maximum run-up (R_{max}) comparison for XB-NH (blue) and XB-**
961 **SB (red) with default (*maxbrsteep = 0.6, alpha = 1*) and calibrated (*maxbrsteep = 0.5, alpha = 1.4*)**
962 **parameter values showing SCI and Relative Bias error values (Buckley et al. [17] experiment).**
963 **Black solid lines represent perfect agreement. Black dashed lines represent +/− 25% error.**

964

965

966

967

968

969

970

971

972

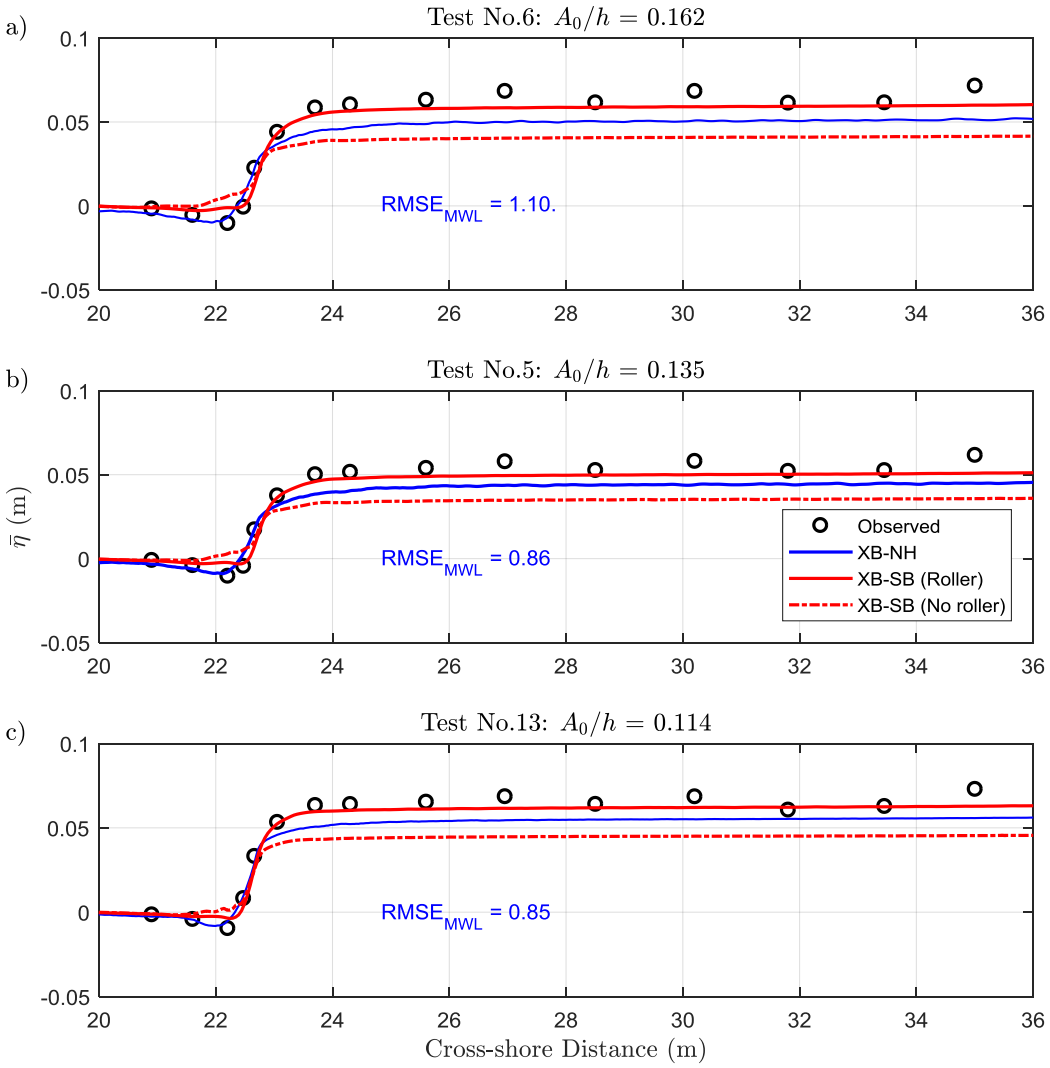

Figure 14 Modelled and observed mean water level ($\overline{\eta}$) profiles for tests no. (a) 5, (b) 6 and (c) 13 which showed the highest nonlinearity (A_0/h) and root-mean-square error in mean water level predictions ($RMSE_{MWL}$) for XB-NH (blue), XB-SB with roller model (red solid) and XB-SB without roller model (red dash-dot). Note: A_0 = offshore wave amplitude ($H_{m0}/2$) and h = offshore water depth.

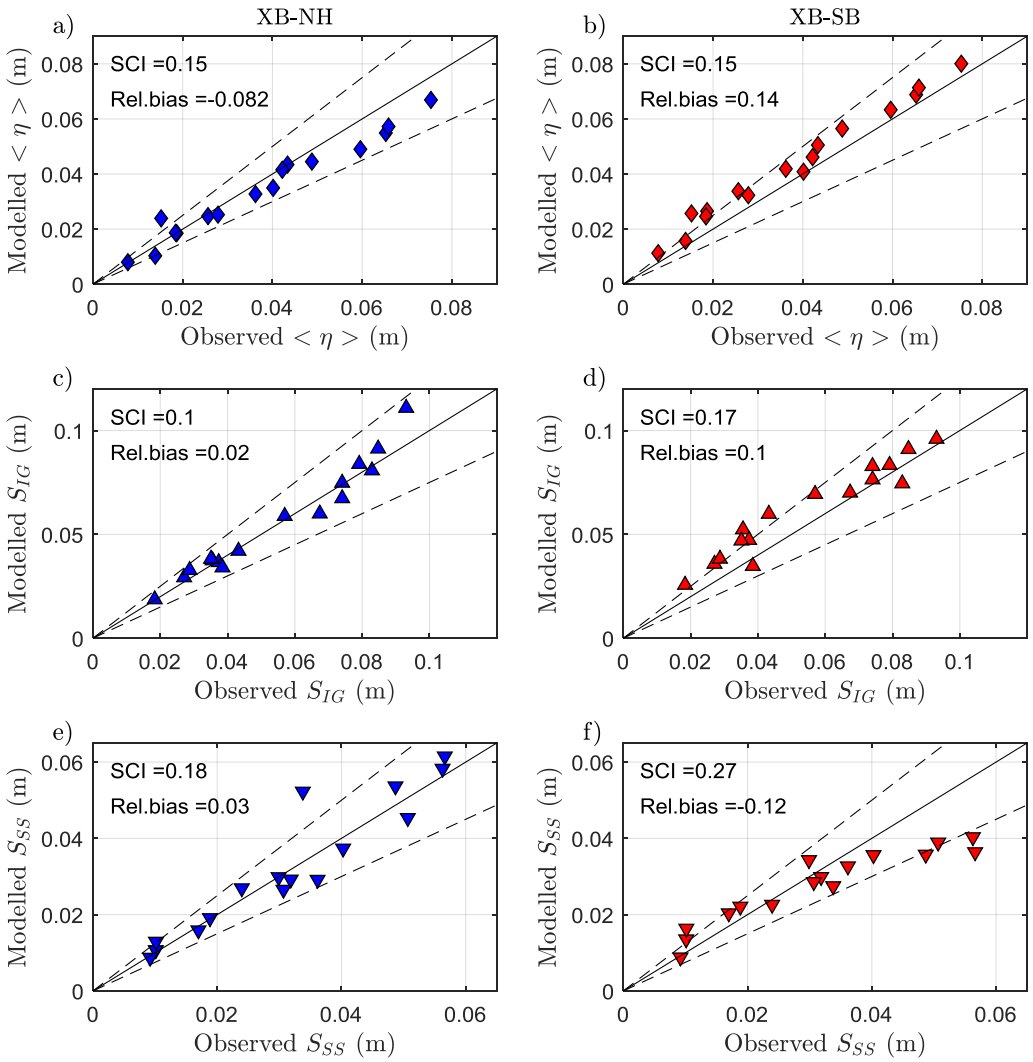

980

981 **Figure 15 Modelled and observed (a, b) shoreline setup, (c, d) infragravity-band swash and (e, f)**
982 **sea-swell band swash for all 16 tests (Buckley et al. [17] experiment) for XB-NH (blue) and XB-**
983 **SB (red) showing SCI and Rel. bias error values.**

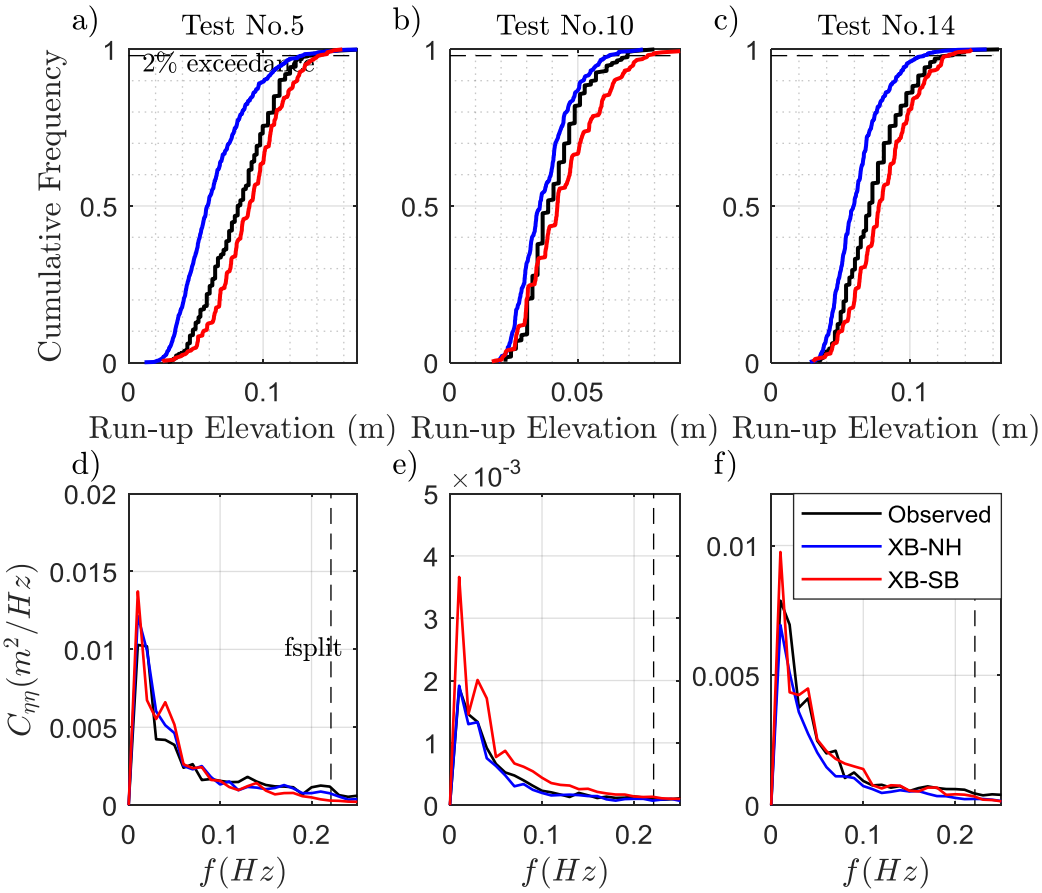

984

985 **Figure 16 Modelled and observed cumulative frequency curves (upper) and swash spectra (lower)**
986 **for representative tests no. (a, d) 5, (b, e) 10 and (c, f) 14 (Buckley et al. [17] experiment) for both**
987 **XBeach modes. Horizontal dashed lines represent 2% exceedance, vertical dashed lines represent**
988 **the split frequency ($f_{split} = fp/2$) and the resolution of the spectra is 0.01 Hz with approximately**
989 **125 degrees-of-freedom.**